Combination of Fluorine and Tertiary Amine Activation in Catalyst-Free Thia-Michael Covalent Adaptable Networks

Dimitri Berne, Rinaldo Poli, Sylvain Caillol, Vincent Ladmiral, Eric Leclerc

Combination of Fluorine and Tertiary Amine Activation in Catalyst-Free thia-Michael Covalent Adaptable Networks

Dimitri Berne[a],* Rinaldo Poli[b,c], Sylvain Caillol[a], Vincent Ladmiral[a], Eric Leclerc[a]*

[a] ICGM, Univ Montpellier, CNRS, ENSCM, Montpellier, France

[b]CNRS, LCC (Laboratoire de Chimie de Coordination), UPS, INP, Université de Toulouse, 31077 Toulouse, France

[c] Institut Universitaire de France, 75231 Paris, France

dimitri.berne@enscm.fr, eric.leclerc@enscm.fr

Abstract

A series of catalyst-free covalent adaptable networks (CANs) has been developed using a reversible thia-Michael reaction activated by fluorine atom substitution and by an intramolecular tertiary amine. The thia-Michael exchange rate was first evaluated by a preliminary molecular study coupled with DFT calculations. This study enabled to highlight the necessity of combining fluorine and tertiary amine activation to observe the thia-Michael exchange. Then, by modulating the structure, nature and functionality of the thiol monomers, a wide range of mechanical properties and thermal properties were achieved. Relationships between the monomer structure and the dynamic properties were also highlighted through the dynamic study of these materials. Finally, the ability of the fluorinated thia-Michael CANs to be reprocessed was assessed by thermal and mechanical analyses up to three reshaping cycles.

Graphical Abstract

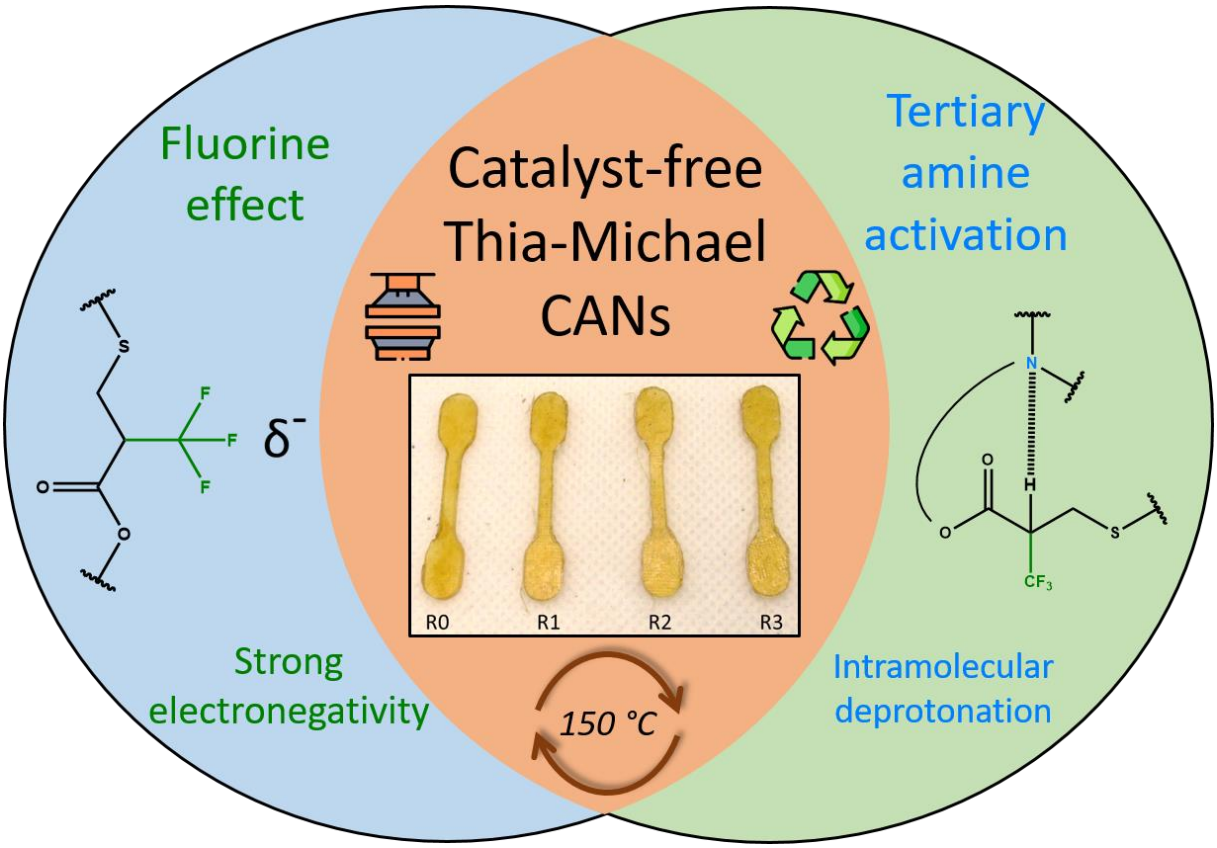

Keywords

Covalent Adaptable Network, Thia-Michael, Tertiary amine, Fluorine activation, Neighboring group participation, DFT calculations

Introduction

The thia-Michael addition has been used for several decades to build C-S bonds, which are fundamental units in organic chemistry.[1] They are essential linkages for a range of pharmaceuticals, pesticides, food additives and surfactants.[2–5] Attracted by its high efficiency, rapidity and selectivity, allowing its qualification as a click reaction,[6] researchers have also employed this synthetic tool for the development of polymer materials.[7,8]

In addition, the introduction of a thia-Michael step in polymer synthesis gave rise to a new kind of dynamic covalent adaptable networks (CANs). Indeed, even though thermosets featuring thia-Michael adducts as structural units did not initially show any dynamic behavior, it was later demonstrated that,

for specific β-thioesters and/or in the presence of certain catalysts (such as DBU),[9,10] a certain degree of reversibility could be achieved. Consequently, depending on the temperature or pH range, bond exchange can occur on thia-Michael adducts, thus conferring dynamic properties to the polymeric networks.[11] For instance, high exchange rates at moderate temperature were reported at the molecular and material levels for maleimide[12–14] or quinone methide[15] systems. Michael exchange was even reported to occur at ambient temperature, without external catalyst, for benzylidenecyanoacetate-derived thia-Michael adduct.[16] Moreover, Rowan *et al.* demonstrated that placing electron-withdrawing groups such as NO_2 on the β-phenyl ring of a benzylidenecyanoacetate-derived thia-Michael adduct favored the retro-thia-Michael reaction in comparison to analogous structures devoid of specific electronic effects.[17] Allowing the equilibrium to shift towards the dissociated state offers control on the dynamic properties since thia-Michael adducts presumably require a reversion to the Michael acceptor to allow exchange with another function.[11] D. Konkolewicz *et coll.* demonstrated that changing the polymerization method from RAFT to conventional radical polymerization in the preparation of thia-Michael CANs decreased the dynamic properties, probably because of the higher dispersity in the second case.[12]

Recently, numerous catalyst-free CANs have emerged with the aim of reducing potential leaching and accelerated ageing risks related to the presence of additives.[18–23] Multiple strategies, including neighboring group participation (NGP), have emerged to improve the exchange rate.[24,25] For example, transesterification in epoxy vitrimers can be accelerated *via* transition state stabilization either by hydrogen bonds[26–31] or by the formation of a cyclic intermediate.[32–36] The use of an excess of exchangeable functions also accelerates the exchange rate and allows the preparation of catalyst-free vitrimers.[37–41] Electron-withdrawing or electron-donating effects of neighboring groups were also demonstrated to be of utmost importance.[19,42,43] This behaviour was reported for CANs based on dioxaborolane exchange, for which electronic effects influence the pKa value of the associated boronic acid and hence the rate of dissociation.[44,45] The nature of the polymer matrix was also shown to be a

critical parameter for the dynamic properties of CANs[46] as well as the steric hindrance of the neighboring groups, which can also play a role on the exchange reaction rate.[47,48]

Finally, an interesting strategy is the incorporation of reactive groups (such as tertiary amine) in the CAN structure, sometimes described as "internal catalysis". In this case, the catalyst needed for the exchange reaction to occur is covalently bonded to the network, preventing any leaching. This strategy has been used to develop CANs based on transesterification,[32,49–54] silyl ether exchange[55–57] or disulfide exchange,[58] where the reactions are internally catalyzed by tertiary or secondary amines. In the case of transesterification vitrimers, the insertion of a tertiary amine was relatively simple as this functionality is already present in commercially available multi-functional epoxides or can easily be obtained by epoxy/amine reaction. In contrast, synthetic steps were required to introduce a tertiary amine in dioxaborolane[59] or silyl ether based networks.[55–57] In addition to their catalytic effect on the exchange reactions, tertiary amines can also promote the network formation. For instance, the epoxy/acid reaction required to prepare certain transesterification vitrimers can be performed under much milder conditions in the presence of tertiary amines.[60–62]

In the last few years, our group has evidenced the significant activating effect of fluorine for the synthesis of a range of polymer networks. In particular, thanks to its high electronegativity, epoxy/acid,[63,64] amidation[65] and Michael additions (including the aza- and thia- versions)[66–68] have been shown to be strongly accelerated by proximal fluorine-atom substitution. Moreover, fluorine activation not only enables the fast synthesis of these networks, but also promotes a series of exchange reactions. Indeed, the use of α-difluorinated[64,69,70] or α-CF_3[63] esters enables the reprocessability of catalyst-free transesterification vitrimers. In depth studies combining kinetics and DFT calculations highlighted the specific activation by fluorine on transesterification[63,64] and transamidation[65] and quantified its impact on the activation energy of the respective exchange reaction.[65,71] Finally, fluorine activation of the recently introduced aza-Michael exchange enabled to drastically decrease the reprocessing temperature of these CANs.[66]

However, if the fluorine activating effect on this series of exchange reaction has been clearly demonstrated, our previously reported thia-Michael thermosets exhibited no dynamic properties in the absence of any internal or external base, despite the presence of a CF_3 group.[67] Indeed, the latter clearly accelerated the thia-Michael reactions and the synthesis of the networks but failed to trigger a reverse reaction on its own. Hence, on the basis of our recent successful development of fluorine-activated catalyst-free CANs, we targeted a series of innovative CANs prepared from the combination of a tertiary amine-functionalized *tris*-(trifluoromethyl)acrylate with a number of multivalent thiols. This approach thus combines the fluorine activation effect and the presence of an internal tertiary amine to promote the thia-Michael exchange. In order to assess the individual impact of each of these activating groups, model molecular reactions were also examined and the various reactive pathways were assessed via DFT calculations. The chemical, mechanical, thermal and dynamic properties of the resulting CANs were also examined.

Results and discussion

Model reactions

The thia-Michael addition of an aryl or alkyl thiol onto a trifluoromethylacrylate was shown to be much faster than the addition to non-fluorinated counterparts.[67] The aim of this preliminary molecular study was to independently determine the impact of a trifluoromethyl group and of a tertiary amine catalyst on the thia-Michael exchange. The effects of the pKa of the amine catalyst as well as its nature (external or internal) were evaluated. In order to complete this study, fluorinated thia-Michael acceptors and adducts were synthesized. First, trifluoromethylacrylate esters **2** and **3** (the latter featuring a tertiary amine function on the side chain) were synthesized *via* a two-step procedure (Scheme 1). Trifluoromethylacrylic acid (MAF) was first converted, *via* the action of phthaloyl dichloride, to its acyl chloride **1**, which was isolated by distillation and then esterified under mild conditions with the desired alcohol. The fluorinated thia-Michael adducts **4** and **5** were easily prepared by the reaction at room temperature of thiophenol with *tert*-butyl trifluoromethacrylate (MAF-TBE) and **3** respectively

(Scheme 2). Ester **6**, the non-fluorinated equivalent of **5,** was synthesized by the thia-Michael addition of thiophenol onto 2-(diethylamino)ethyl acrylate, which also occurred at 25 °C due to the "internal catalysis" of the embedded tertiary amine. The structures of these model molecules **2**, **3**, **4**, **5** and **6** were confirmed by ^{1}H, ^{13}C, ^{19}F-NMR (Figures S1-5) and HR-MS.

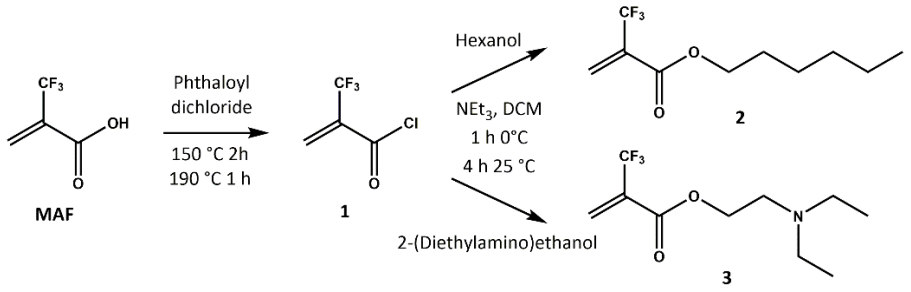

*Scheme 1. Synthesis of hexyl- and 2-(diethylamino)ethyl-(trifluoromethyl)acrylate (**2** and **3** respectively).*

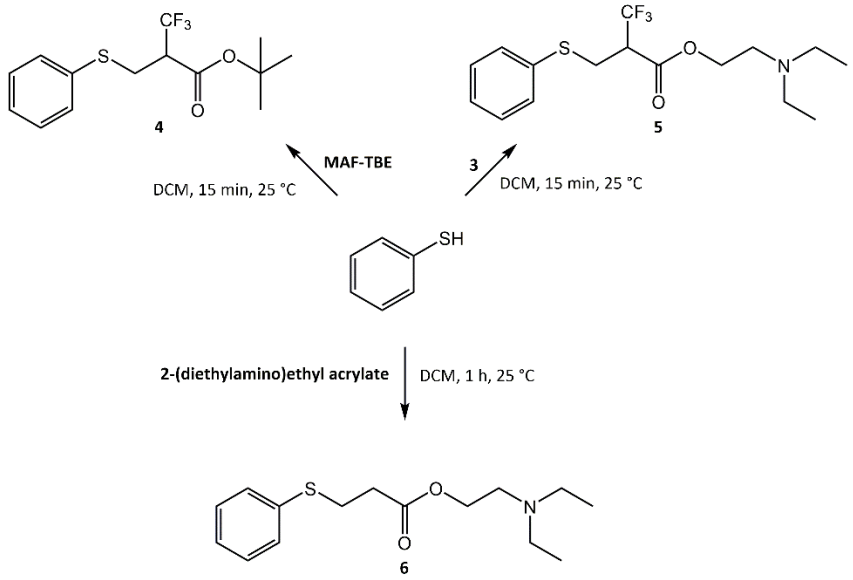

*Scheme 2. Synthesis of thia-Michael adducts **4**, **5** and **6** from thiophenol.*

The fluorine effect on the thia-Michael exchange was first evaluated. One equivalent of **4** was reacted with 10 equivalents of **2** either under catalyst-free conditions or in the presence of tribenzylamine (1 eq.) or DBU (1 eq.) (Scheme 3A). The exchange conversions were monitored by GC-MS according to the **4**/**7** peak ratio; the results are reported in Table 1. As expected from our previous work regarding fluorinated thia-Michael thermosets, [67] no exchange was detected in the absence of catalyst at 100 °C for 24 h, confirming the non-reversibility of the thia-Michael reaction in the absence of base and despite the presence of an activating group. A similar result was obtained using tribenzylamine as a

weak external base while DBU proved much more efficient as a catalyst since significant exchange occurred after 5 h in its presence. The latter base has been previously used as a catalyst in other thia-Michael exchange processes,[10,72] but its toxicity and volatility (boiling point 260 °C) could be seen as inconvenient for CAN applications. The difference in reactivity between tribenzylamine and DBU was attributed to their pKa difference (6.9 and 13.3 respectively). Indeed, DBU acts as a strong base and presumably accelerates the dissociation of the thia-Michael adduct by facilitating the elimination reaction, as well as the Michael addition step by deprotonation of the thiol.[11] At 150°C, tribenzylamine moderately promoted the thia-Michael exchange, but no exchange was detected in the absence of catalyst even after 48 h. Following these first experiments, the influence of an embedded tertiary amine was evaluated by reacting **5** with excess **2** (Scheme 3B). In this case, almost complete conversion of **5** into **7** was achieved after 5 h at 100 °C. In contrast, the non-fluorinated analog **6** (Scheme 3C) did not react even at 150 °C after 24 h. These results highlight the importance of both the amine catalyst (its pKa but also its inter- or intramolecular action) and the role of fluorine activation on reactivity. Indeed, the experimental results suggest that the internal tertiary amine facilitates the retro-thia-Michael reaction. The proximity of the amine moiety with the proton α to the CF_3 group might allow the elimination reaction to proceed through a concerted, cyclic transition state. Thanks to this intramolecular process, the weaker basicity of the tertiary amine compared to DBU seems nevertheless sufficient to trigger the retro-thia-Michael reaction. In addition, the electron-withdrawing CF_3 group clearly activates the thia-Michael exchange, presumably by increasing the acidity of the α-proton, since no exchange occurred in the non-fluorinated series.

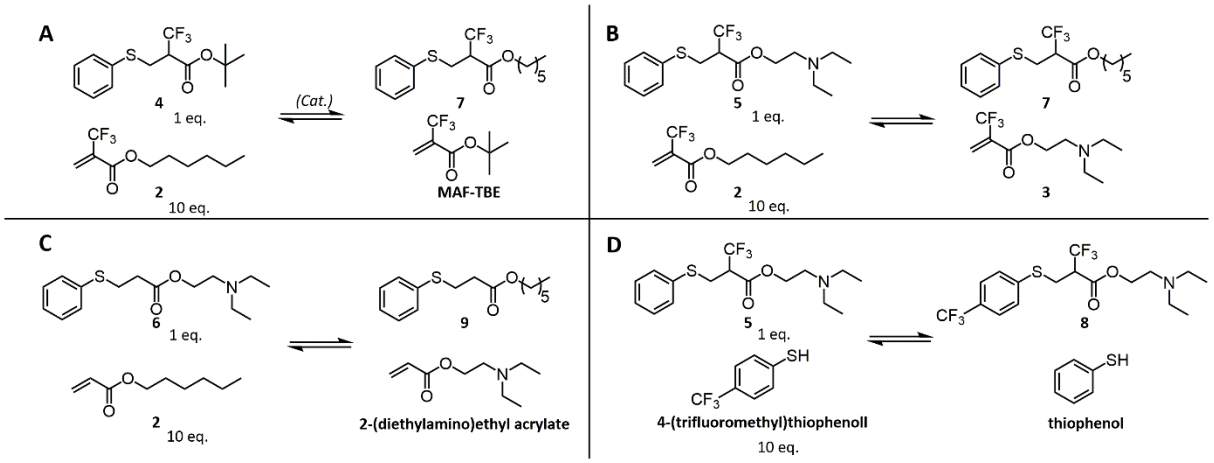

Scheme 3. Exchange reactions of fluorinated and non-fluorinated thia-Michael adducts with Michael acceptors or donors.

Table 1. Quantitative results of the exchange reactions presented in Scheme 3.

Exchange reaction	Temperature (°C)	Time (h)	Exchange ratio
A-No catalyst	100	24	100/0 (**4**/**7**)
A-No catalyst	150	48	100/0 (**4**/**7**)
A-Cat = tribenzylamine	100	24	100/0 (**4**/**7**)
A-Cat = tribenzylamine	150	10	76/24 (**4**/**7**)
A-Cat = DBU	100	5	2/98 (**4**/**7**)
B	100	5	1/99 (**5**/**7**)
C	100	24	100/0 (**6**/**9**)
C	150	24	100/0 (**6**/**9**)
D	100	5	5/95 (**5**/**8**)

Finally, an additional exchange reaction was carried out between **5** and an excess of 4-(trifluoromethyl)thiophenol as a Michael donor (Scheme 3D). Similar conversion rates to the reaction of **5** with an excess of Michael acceptor **2** (Scheme 3B) were obtained. These observations are consistent with the dissociative nature of the thia-Michael exchange.

DFT calculations

The neighboring CF_3 effect in the thia-Michael addition of PhSH (thiophenol) to CH_2=C(CX_3)COOMe (X = H, F), abbreviated respectively as **MMA** and **MMAF**, has already been the subject of a recently reported DFT investigation.[67] The reaction mechanism involves the conjugate 1,4 addition of the S-H bond *via* a 6-membered transition state, yielding the Ph$SCH_2C(CX_3)$=C(OH)(OMe) ester enol intermediate, which then tautomerizes to the more stable Ph$SCH_2CH(CX_3)$(COOMe) ester product. The

transition state Gibbs energy, relative to the separate reagents, is decreased from 21.6 to 15.8 kcal mol^{-1} when the methacrylate CH_3 group is replaced with CF_3. These energy profiles are recalled for convenience in Figure S6. For a dissociative exchange to occur, the thia-Michael addition adduct must follow the reverse pathway to regenerate the separate methacrylate and thiol functions. Thus, in spite of the electronic assistance of the CF_3 group, the process still needs to overcome an activation barrier of 23.8 kcal mol^{-1} for the reverse S-C cleavage and is thus substantially more difficult than the forward process.

In order to assess the catalytic effect of an added amine, additional calculations were carried out with the explicit inclusion of an amine molecule. For comparison purposes, the calculations were carried out using the same DFT method and corrections as in the already published catalyst-free thia-Michael addition (see computational details).[67] The intermolecular version of the catalyzed reaction was investigated first, using NMe_3 as a computational model for the tribenzylamine used in the experiment.

An initial investigation probed the amine ability to deprotonate the various compounds, namely PhSH, the enol intermediates $PhSCH_2C(CX_3)=C(OH)(OMe)$ and the final products $PhSCH_2CH(CX_3)COOMe$ (X = H, F). The results of the calculations (Figure S7) indicate that thiophenol is spontaneously deprotonated to yield the $PhS^-HNMe_3^+$ salt, held as a contact ion pair by an N-H···S hydrogen-bond (1.933 Å), with a Gibbs energy gain of -1.4 kcal mol^{-1}. This qualitatively agrees with the stronger acidity of the thiophenol (pK_a 6.62) than the conjugate acid of trimethylamine (pK_a 9.8), although those values refer to the aqueous medium while the calculations were done in a polarizable medium with ε = 4.5. Note that tribenzylamine, though less basic that trimethylamine (pK_a of the conjugate ammonium salt = 6.90) is still sufficiently basic to undergo a deprotonation equilibrium with PhSH in water. The enol molecules are even more favorably deprotonated, with Gibbs energy gains of -11.6 (X = H) and -13.1 (X = F) kcal mol^{-1}. Thus, there is greater stabilization of the enolate in the presence of the electron-withdrawing CF_3 group, as expected. The H-bonding interaction, however, is stronger in the non-fluorinated derivative (N-H···O = 1.451 Å) than in the fluorinated one (1.604 Å), which is also expected. Finally, the

interaction of the thia-Michael product with NMe_3 shows a stark difference for the two derivatives: when X = F, the compound can transfer the C-H proton to the amine to yield the ammonium enolate as a contact ion pair (N-H···C = 1.853 Å), although this proton transfer is endoergic (+10.0 kcal mol^{-1}). When X = H, on the other hand, no stable minimum for a corresponding enolate salt could be located, the structure optimizing as the thia-Michael ester adduct with a rather loose H-bond between the α-CH atom and the amine (C-H···N = 2.122 Å). This van der Waals adduct is located at +4.6 kcal mol^{-1} from the two separate molecules. Incidentally, while reoptimizing the two thia-Michael adducts, $PhSCH_2C(CX_3)COOMe$ (X = H, F) in the course of the present investigation, new minima were located at lower G than those reported in our previous publication (*cf.* Figure 1 and Figure S6).[67]

The full pathway of C-S bond formation and breaking has subsequently been explored in detail for the combination of PhSH/MMAF/NMe_3, as shown in Figure 1. In the bond breaking direction (from right to left), the first step is the endoergic α-CH deprotonation already analyzed above, which brings the system from the product (**P**) plus catalyst at -14.3 kcal mol^{-1} to the the $(PhSCH_2)(CF_3)(COOMe)C^-\cdots HNMe_3^+$ contact ion pair at -2.2 kcal mol^{-1} (**D**), via an optimized transition state $\mathbf{TS_{DP}}$ that has a barely higher electronic energy, but a lower Gibbs energy (-4.3 kcal mol^{-1}) than the contact ion pair, indicating that the C-H bond formation from the salt is an essentially barrier-less process. A shift of the cation from the negatively charged C atom to the O atom of the enolate anion yields the $(PhSCH_2)(CF_3)C(COMe)O^-\cdots HNMe_3^+$ contact ion pair (**C**) at -0.6 kcal mol^{-1} and proceeds *via* a very low barrier ($\mathbf{TS_{CD}}$ at 1.4 kcal mol^{-1}). Next, to prepare for the C-S bond breaking, the ammonium cation is further shifted from the enolate O atom to the S atom to yield $(Me_3NH^+\cdots PhS^-CH_2)(CF_3)C(COOMe)$ (**B**) at -1.1 kcal mol^{-1} via another quite low transition state ($\mathbf{TS_{BC}}$ at 0.7 kcal mol^{-1}). The final step is the ammonium-assisted retro-1,4-conjugate addition, producing MMAF and the $PhS^-\cdots HNMe_3^+$ contact ion pair (**A**). This occurs *via* the highest energy (rate-determining) transition state $\mathbf{TS_{AB}}$ at 3.2 kcal mol^{-1}, which is however still quite low relative to the TS of the uncatalyzed pathway (15.8 kcal mol^{-1}). Thus, the key action of the amine for both the thia-Michael addition and its reverse is to generate stronger nucleophiles *in situ*, facilitating the C-S bond formation and its microscopic reverse.

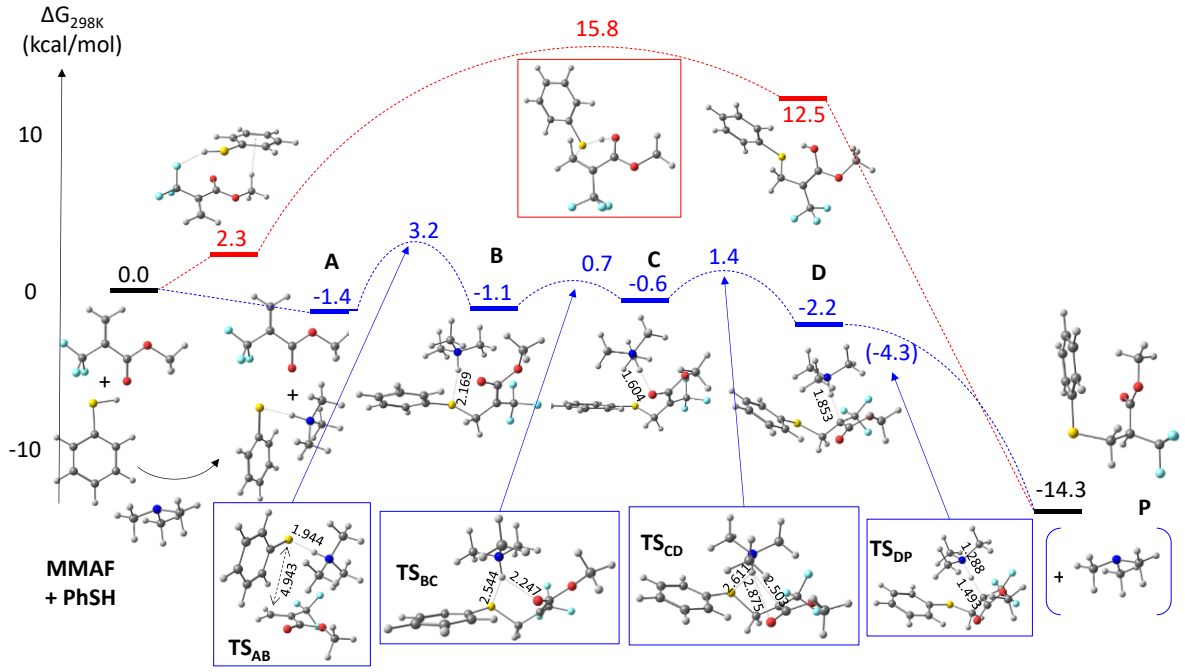

Figure 1. Gibbs energy profile of the thia-Michael addition of PhSH to CH_2=C(CF_3)COOMe, at 298 K in a polarizable continuum with ε = 4.5, with and without the catalytic action of NMe_3.

The investigation of the corresponding pathway for the non-fluorinated analog was less detailed, analyzing only the local minima. The inability of NMe_3 to deprotonate the ester product is an immediate hint of the greater difficulty for the retro thia-Michael addition in the regular methacrylate system. The relative energy of the ammonium enolate contact ion pair, $(PhSCH_2)(CH_3)C(OMe)O^-\cdots HNMe_3^+$, places this compound at +10.0 kcal mol^{-1} relative to the separate MMA and PhSH reagents plus NMe_3 catalyst and at +20.0 kcal mol^{-1} relative to the thia-Michael addition product (see Figure S8). Therefore, obtaining the ammonium enolate intermediate by deprotonation of the ester product, though less difficult than tautomerizing in the absence of amine, remains much less favorable than the corresponding process for the fluorinated analogue. To complete the retro-thia-Michael addition, a shift of the ammonium cation from the O to the S atom yields, in this case, direct C-S bond cleavage to generate a van der Waals adduct of MMA with the $PhS^-\cdots HNMe_3^+$ contact ion pair, located at +2.9 kcal mol^{-1} (Figure S8). The calculations therefore clearly show how the external NMe_3 catalyst promotes the retro-thia-Michael addition much more favorably for the CF_3-activated system.

Since it has been shown that a stronger base (*e.g.* DBU) is able to activate the reversible thia-Michael addition to regular acrylates,[73] the intermediates along the thia-Michael addition pathway for the PhSH/MMA system have also been calculated in the presence of DBU. The results are also shown in Figure S8. In this case, a local minimum could indeed be optimized for the $(PhSCH_2)(CH_3)(COOMe)C^-\cdots HDBU^+$ contact ion pair (2.0 kcal mol^{-1} higher than PhSH + MMA + DBU and 12.0 kcal mol^{-1} higher than the final thia-Michael adduct $PhSCH_2C(CH_3)COOMe$ + DBU). The cation migration from C to O yields a contact ion pair $(PhSCH_2)(CH_3)C(OMe)O^-\cdots HDBU^+$ of nearly identical energy (2.1 kcal mol^{-1}), much lower than the free enol (the enol deprotonation is exoergic by -16.7 kcal mol^{-1}). Therefore, all intermediates along the thia-Michael C-S bond formation and reverse bond cleavage are greatly stabilized (Figure S8), though not as much as those of the corresponding fluorinated system in the presence of the weaker NMe_3 base.

Finally, the DFT tool was also used to assess the greater ability of the internal amine function, relative to an external one, to catalyze the retro-thia-Michael reaction. A simplified model was again used, with the $-CH_2CH_2NEt_2$ acrylate substituent replaced by $-CH_2CH_2NMe_2$. The basicity of this internal amine function is similar to that of the external NMe_3 used as model for the above calculations. The interaction between the $CH_2=C(CF_3)COOCH_2CH_2NMe_2$ acrylate (named **MMAF-NMe$_2$**) and PhSH leads, once again, to deprotonation and formation of the $CH_2=C(CF_3)COOCH_2CH_2NHMe_2^+SPh^-$ contact ion pair (**E**), with a Gibbs energy gain of -3.2 kcal mol^{-1} (Figure 2). This intermediate then leads to a facile nucleophilic addition of the thiolate to the acrylate C atom, *via* the transition state **TS$_{EF}$** located only at 0.6 kcal mol^{-1} relative to the separate reagents. The lower energy of this transition state with respect to that of the intermolecular addition of $PhS^-HNMe_3^+$ can be ascribed to the lower entropy penalty associated to the reorganization leading to the C-S bond formation. Indeed, according to the calculation, the $\Delta S^{\ddagger}_{298}$ for this transition state (relative to the separate reagents) is -50.6 cal mol^{-1} K^{-1} ($-T\Delta S^{\ddagger}_{298}$ = 15.1 kcal mol^{-1}), whereas the $\Delta S^{\ddagger}_{298}$ for the corresponding transition state of the C-S bond formation catalyzed by external NMe_3 is -81.6 cal mol^{-1} K^{-1} ($-T\Delta S^{\ddagger}_{298}$ = 24.3 kcal mol^{-1}). The enthalpic activation, on the other hand, is greater for the internal amine, given the strain associated to the

needed reorganization of the aminoethyl arm. The step leads directly to the ammonium enolate **F**, with the ammonium function establishing an intramolecular H-bond to the enolate O atom, located at -4.8 kcal mol^{-1} relative to the separate reagents and -1.6 kcal mol^{-1} relative to the intermediate thiolate salt.

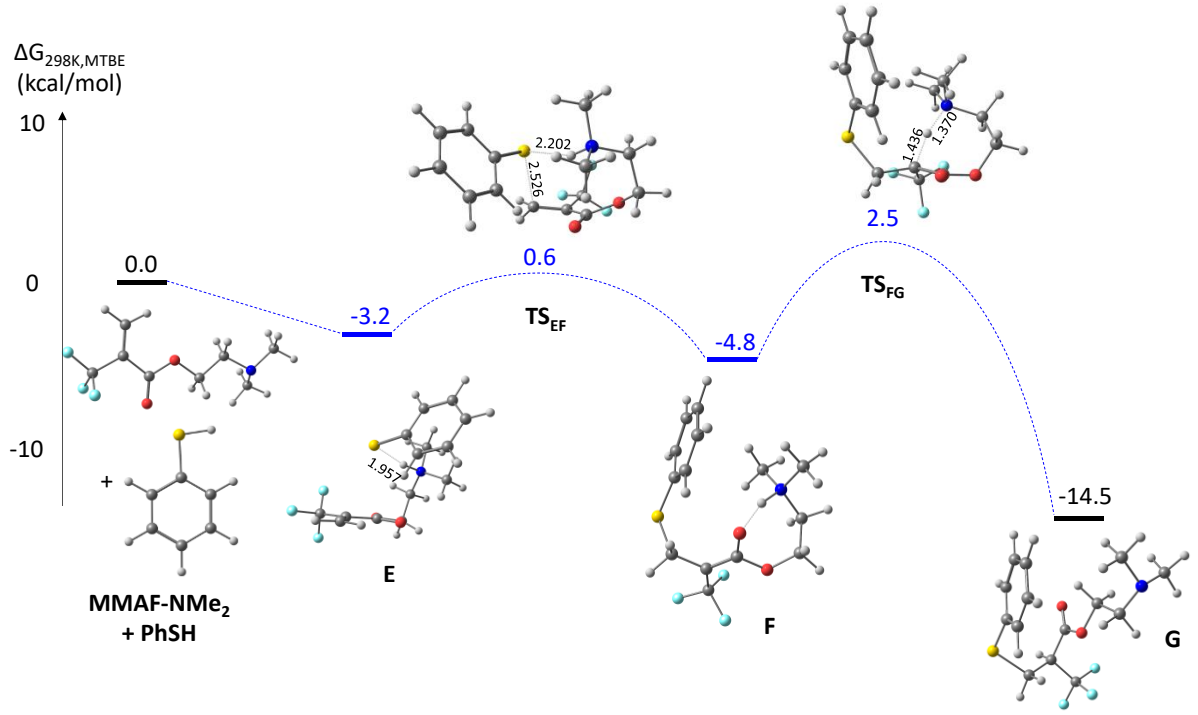

Figure 2. Gibbs energy profile of the thia-Michael addition of PhSH to CH_2=C(CF_3)$COOCH_2CH_2NMe_2$, at 298 K in a polarizable continuum with ε = 4.5.

From the enolate intermediate, the final thia-Michael adduct **G** is obtained by shift of the NH bond from the O atom to the C atom and concerted proton transfer, *via* the rate-determining transition state **TS_{FG}** at 2.4 kcal mol^{-1} from the separate reagents. The thermodynamic gain associated to the C-S bond formation (-14.5 kcal mol^{-1}) is essentially identical to that of the NMe_3-catalyzed addition of PhSH to MMAF, as expected. Along the reverse C-S bond breaking process, the action of the internal amine is thus a lowering of the overall activation barrier, from 17.5 kcal mol^{-1} for the catalytic action of the external amine (from the thia-Michael adduct to the C-S bond breaking transition state, Figure 1), to 17.0 kcal mol^{-1}, the rate-determining step now becoming the deprotonation step.

Thia-Michael networks synthesis

Once the dynamic character of the thia-Michael adduct under the dual activation by fluorine and tertiary amine was demonstrated, seven CANs based on this exchangeable bond were synthesized. First, a trifunctional (trifluoromethyl)acrylate incorporating a tertiary amine (**$NMAF_3$**) was synthesized from triethanolamine as previously reported.[68] Reacting **$NMAF_3$** with 1,3-propanedithiol, 1,4-butanedithiol, 1,5-pentanedithiol, 1,6-hexanedithiol, 2,2'-(ethylenedioxy)diethanethiol, pentaerythritol tetrakis(3-mercaptopropionate) and 4,4'-thiobisbenzenethiol, led to the corresponding thia-Michael CANs (**TMCANs**): **Prop-**, **But-**, **Pent-**, **Hex-**, **EDT-**, **PETMP-** and **TBT-TMCAN**, respectively (Figure 3). This network formation reaction was carried out in solution (50 wt% in DCM) as the thia-Michael addition was extremely fast and exothermic at 25 °C in the absence of solvent. Indeed, the presence of the tertiary amine drastically accelerated the addition compared to the previously reported non-catalyzed fluorinated system (curing at 50 °C for 10 h).[67] The **TMCANs** were obtained *via* a solvent casting process (24 h at 25°C and then under vacuum at 50 °C for 10 h). However, the shape of the resulting materials could not be easily controlled by this method. Hence, a last curing step consisted of the shaping of the materials using a hot press. All **TMCANs** were treated at 150 °C for 1 h under 3 t, excepted for **TBT-TMCAN,** which could be shaped at 120 °C under otherwise identical conditions.

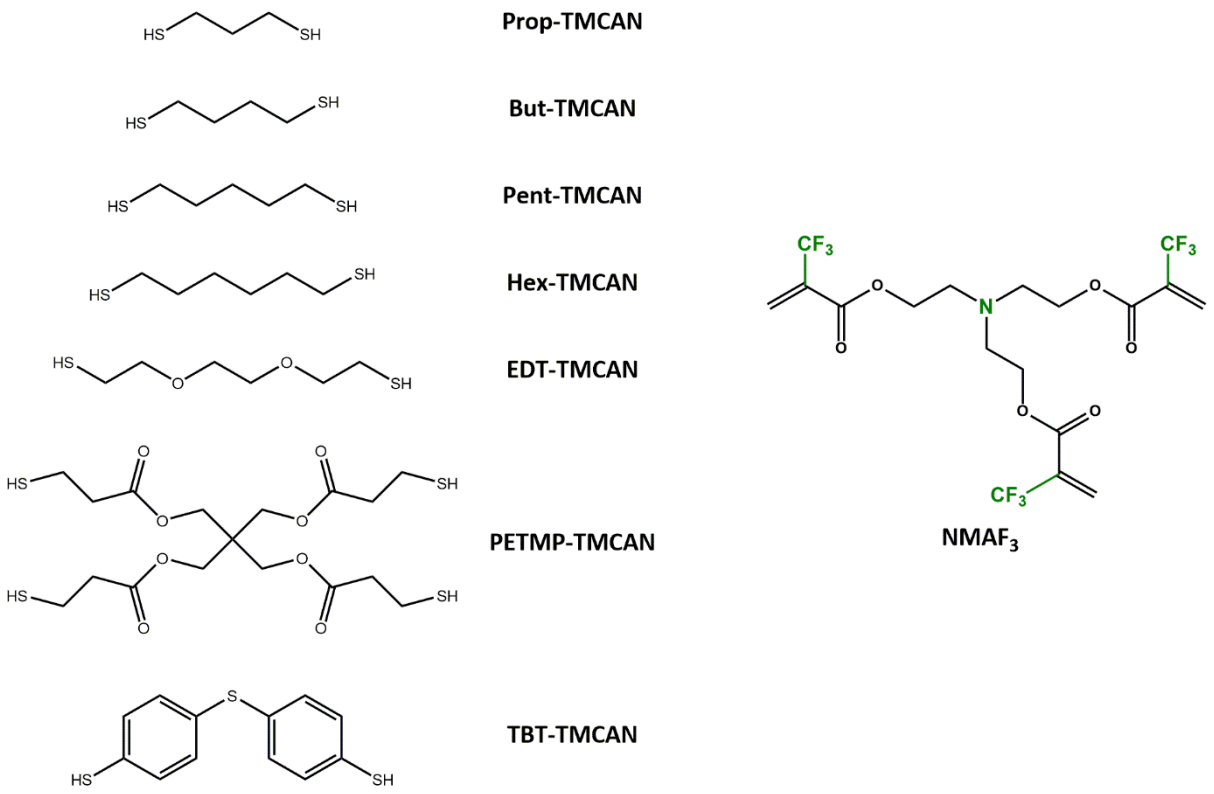

*Figure 3. Structure of the monomers employed for the synthesis of **TMCANs** (associated to their acronyms). Figure*

In order to confirm the formation of a cross-linked network for all **TMCANs** and compare their mechanical and chemical properties, several analyses were performed (Table 2). The high gel contents in THF (> 80%) measured for all the samples confirmed the 3D structure. Swelling indexes were not significantly different between **Prop**, **But**, **Pent**, **Hex** and **EDT-TMCANs** as their structure were relatively similar. However, **PETMP** and **TBT-TMCANs** showed lower swelling indexes and slightly higher gel contents compared to the other **TMCANS**. In the case of **PETMP-TMCAN**, this probably results from the higher **PETMP** functionality, yielding a more densely crosslinked network, whereas the results for **TBT-TMCAN** may be ascribed to the fact that the measurements were carried out below its glass transition (T_g = 30 °C). The specific chemical composition of these two networks may also be one reason to explain this difference of solvent affinity. The FTIR analysis (Figures S9-10) confirmed the quantitative incorporation of the (trifluoromethyl)acrylate functions, since the characteristic C=C stretching band of **NMAF₃** (1651 cm^{-1}) and the S-H stretching band (2556 cm^{-1}) of the thiol monomers were no longer detected in the FTIR spectra of the cured materials, as shown in Figure S9. Critical degradation (5 % weight loss) occurred above 230 °C for all the samples. The **TMCANs** thus offer a wide

range of operating temperatures (Figure S11). The lower thermal stabilities observed for **EDT-TMCAN** and **PETMP-TMCAN** can be due to the presence of ether and ester functions in **EDT** and **PETMP** respectively. The lower $Td^{5\%}$ for the degradation of **TBT-TMCAN** compared to the other materials may indicate a faster dissociation of thia-Michael adducts based on thiophenols. The DSC analysis performed from -100 °C to 150 °C confirmed that all the **TMCANs** were fully cured as no residual exothermic peaks were observed (Figure S12). Such a wide range of thiophenol monomers allowed to tune the T_g of the resulting **TMCANs** from -19 °C to 30 °C. Finally, temperature sweeps performed on a DMA instrument allowed the determination of the glassy and rubbery storage moduli as well as the alpha transition temperatures (T_α) (Table 2 and Figure S13).

Table 2. Results of the TGA, DSC, DMA and insolubility test analyses.

Material	GC (%)[a]	SI (%)[a]	$Td^{5\%}$ (°C)[b]	T_g (°C)[c]	T_α (°C)[d]	E'_{glassy}[e] (GPa)	$E'_{rubbery}$[f] (MPa)
Prop-TMCAN	80 ± 3	133 ± 35	275	-9	-2	4.4	2.7
But-TMCAN	85 ± 2	106 ± 25	272	-15	-9	1.8	2.2
Pent-TMCAN	80 ± 3	137 ± 20	282	-17	-12	1.3	1.9
Hex-TMCAN	81 ± 1	180 ± 32	281	-19	-16	3.3	1.3
EDT-TMCAN	85 ± 3	170 ± 9	229	-15	-7	2.7	1.3
PETMP-TMCAN	87 ± 3	82 ± 10	240	17	25	1.9	10.1
TBT-TMCAN	25 ± 7	92 ± 2	237	30	39	2.3	7.2

[a]Gel content and swelling indexes measured after a 24 h immersion in THF at 25 °C; [b]Temperature of degradation corresponding to 5 % weight loss determined by TGA; [c]Glass transition temperature determined by DSC, [d]α transition temperature determined by DMA at E'' maxima; [e]Determined at T_α – 50 °C; [f]Determined at T_α + 50 °C.

Several considerations can be made on the results shown in Table 2. First, the transition temperature from the glassy to the rubbery state and the value of $E'_{rubbery}$ increase as the number of carbon atoms in the dithiol precursor chain decreases. Indeed, as the length of this carbon chain decreases, the crosslink density rises, leading to a rise of the mechanical properties as well as a reduction of the chain

mobility. The glassy storage modulus did not seem to follow a specific trend, indicating that the thiol crosslinker has a lower impact on the glass mechanical properties. Especially high rubbery storage modulus (10.1 MPa) and T_g (17 °C) values were observed for **PETMP-TMCAN**. In this case, the tetravalence of **PETMP** led to the formation of a highly crosslinked network with limited chain mobility compared to the other materials. Regarding **TBT-TMCAN**, the presence of the two aromatic groups in the monomer structure induced the formation of a network with an even higher glass transition temperature (T_g = 30 °C) and a high storage modulus ($E'_{rubbery}$ = 7.2 MPa).

Dynamic properties

The CAN dynamic properties have been shown to depend not only on the exchange reaction but also on other factors such as the polymer matrix, the catalyst employed and its concentration, or the concentration of the exchangeable functions.[24] In the present study, seven CANs based on a range of dithiols were evaluated by stress relaxation analyses. The temperature window was adapted to each **TMCAN** to maintain the relaxation time in the 10^1-10^4 s range. The temperature-dependent relaxation curves of **EDT-TMCAN** are presented as an example in Figure 4A (for those of the other materials, see Figure S14). Fitting with an extended exponential law ($G/G_0 = \exp(-\tau/t)^{\beta}$) provided the relaxation times, which were then analyzed in an Arrhenius plot (Figure 4B and Table S2).

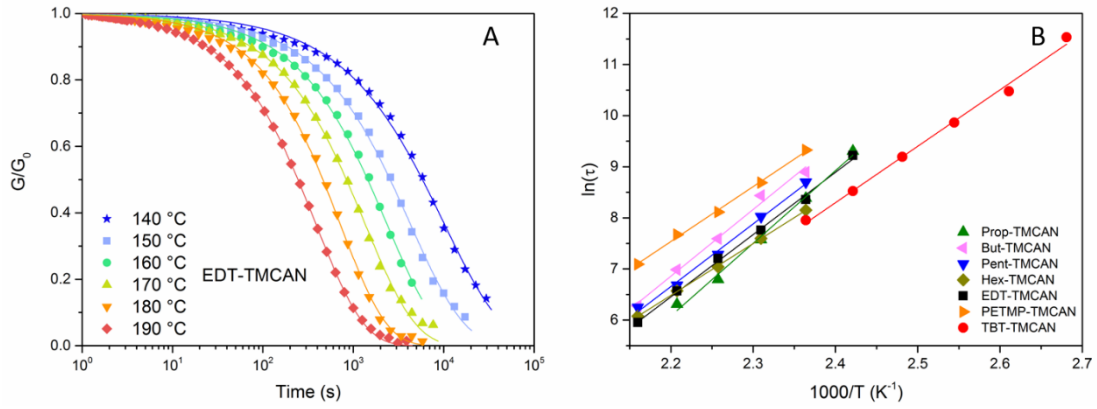

*Figure 4. A) Normalized stress relaxations for **EDT-TMCAN** and B) Arrhenius plot of **TMCANs**.*

All **TMCANs** followed an Arrhenius law in the examined temperature ranges, despite the dissociative nature of the thia-Michael exchange. Although this Arrhenius behavior, typical of vitrimers, was

originally considered as an exclusive feature of associative CANs, it has also been demonstrated for several dissociative CANs.[74] Indeed, an Arrhenius behaviour was also reported for CANs involving a Diels-Alder exchange,[75,76] trans-*N*-alkylation[77] or aza-Michael exchange,[78,79] all occurring through a dissociative mechanism. The highest relaxation times were obtained for **PETMP-TMCAN**, as expected given the higher cross-link density observed for this material compared to the other **TMCANs**. An increase of cross-link density induces a gain of viscosity due to the reduction of the chain mobility, translating into a rise of relaxation time. A similar impact of the crosslink density had already been observed on materials based on dioxaborolane exchange,[80] transesterification[81,82] or vinylogous urethane exchange.[46] The temperature influence on the material viscosity, represented by the flow activation energy value (E_a), was proven to depend on a multitude of factors and is thus difficult to control. Nevertheless, a trend emerges from the comparison of **Prop-**, **But-**, **Pent-** and **Hex-TMCANs**. An increase of the carbon chain length leads to a decrease of the flow activation energy (Table S2). The addition of CH_2 in the dithiol monomer backbone implies a decrease of the resulting material crosslink density, which in the present study has a measurable impact on the flow activation energy. This observation highlights a possible control of the flow activation energies *via* network design.

Recyclability

Once the dynamic character of the **TMCANs** was demonstrated by the stress relaxation analyses, the reprocessing capability of the materials was assessed. After visual optimization trials, all **TMCANs** were reprocessed by hot press at 150 °C for 1 h under 3 t, except for **TBT-TMCAN,** which could be reprocessed at 120 °C in 1 h under 3 t. Figure S15 shows **EDT-TMCAN** after 1, 2 and 3 reprocessing cycles. No color difference or imperfect reprocessing was detected on the materials under these reshaping conditions. The possibility to recycle **TBT-TMCAN** at a lower temperature was anticipated, as this material showed fast stress relaxation compared to the other **TMCANs**. Moreover, thiophenols have already demonstrated higher addition rates than alkylthiols in a previous study[67] and are

expected, due to their lower basicity, to undergo a faster elimination reaction as well. The acceleration of both reactions should result in a global faster exchange than with their alkanethiol analogues.

The chemical and mechanical properties of the pristine **TMCANs** (R0) were compared to those measured after one, two and three cycles (R1, R2 and R3 respectively). The results of TGA, DSC, insolubility tests, DMA and tensile tests are reported in Table S3 and tensile tests results are represented in Figure 5. The FTIR analyses (Figure S10) of the R0-3 **TMCANs** indicated that the chemical integrity of the network was maintained during reprocessing and that no major side reactions occurred during the hot press treatment. No significant changes of the gel contents and swelling ratios were noticed, further indicating that the network structure of the reshaped materials was not significantly affected by the reprocessing protocol. The TGA traces of the reprocessed **TMCANs** (Figure S11) were almost identical to the initial ones, and the same is true for the 5% degradation temperatures (Table S3). The thermal stability of the materials was preserved after reprocessing. In addition, DMA analyses did not highlight any trends in the evolution of the glassy and rubbery storage moduli upon reprocessing (Figure S13). A slight T_α increase (2-7 °C), however, is observed between R0 and R3. The same evolution is also noticeable for the T_g on the DSC thermograms (Figure S12). These trends may be ascribed to structure modifications (such as thioester formation) that could occur after several hours at 150 °C. For **TBT-TMCAN**, the T_g and T_α were less affected by the reprocessing, probably because this sample was reshaped at a lower temperature (120 °C), thus probably limiting the extent of the phenomena causing the increase of the transition temperatures observed on the other **TMCANs**.

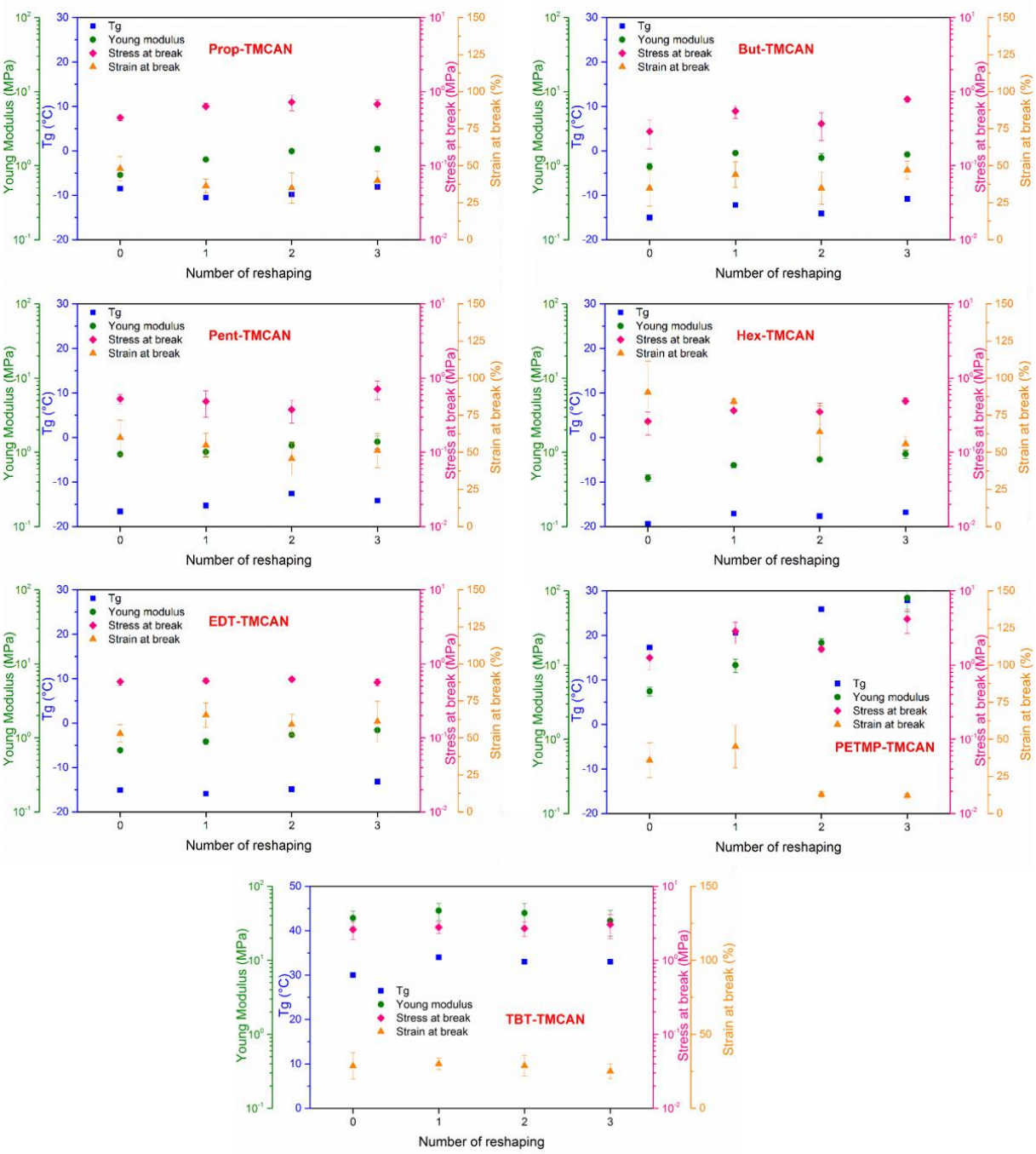

*Figure 5. Tensile tests results and Tg of the initial **TMCANs** and after one, two and three reprocessing cycles.*

The tensile tests results (Figure 5) for **Prop**, **But**, **Pent**, **Hex** and **EDT-TMCAN** followed a similar trend, with a slight increase of the Young modulus and of the stress at break, whereas the strain at break did not significantly change after reprocessing. These slight changes may be caused by some network modification (possible formation of thioesters,[83] for instance) during the heat treatment or by some minor thermal degradation, not detected by the FTIR analysis. In the case of **PETMP-TMCAN**, the

changes were more pronounced, particularly between R1 and R2. This observation is mainly due to the fact that the glass transition is raised above 25 °C (temperature of the tensile analysis) after the second reprocessing cycle. In consequence, R2 and R3 were not tested in their rubbery state but rather in their glassy state, which strongly impacts the mechanical properties. The T_g increase detected for **PETMP-CAN** was slightly higher than for the other **TMCANs,** potentially because this material is more prone to thermal degradation, because of the presence of ester groups. For **TBT-TMCAN**, better mechanical properties were measured as the material was in its glassy state during the tensile analysis (25 °C). The precision of the tensile test was thus significantly reduced as this analysis is more suitable to analyze polymers in their rubbery state. However, according to the collected data, no clear trend was detected for the mechanical properties between the subsequently reprocessed samples of **TBT-TMCAN**. Once again, the lower temperature required to reshape this material likely limited the phenomena potentially responsible for the property changes and allowed the preservation of a very high reprocessability.

The comparison of the mechanical properties of the different TMCANs reveals a decrease of the strain at break as the carbon chain of the dithiol monomers is shortened (from **Hex-** to **Prop-TMCANs**). This is again likely caused by the above-mentioned increase of the crosslink density, which limits the maximal network deformation. Nevertheless, this change did not significantly affect the Young modulus or the strain at break of these TMCANs. As expected, the **PETMP-TMCAN** mechanical properties (for comparable analyses, R0 and R1) were better than those of the other TMCANs, due to its higher crosslink density.

Conclusion

The cumulative effects of combining the strong electron-withdrawing properties of fluorine and the basicity of the tertiary amine to activate the thia-Michael exchange was demonstrated first on molecular model reactions and then in crosslinked materials. The molecular study highlighted, on one hand, the effect of an amine promoter on the thia-Michael exchange rate (using either an

intramolecular or an external amine such as tribenzylamine or DBU) and, on the other hand, the need to activate the acrylate function with a CF_3 group to observe an efficient thia-Michael exchange. DFT calculations confirmed the strong catalytic role of the tertiary amine and the suspected dual activation. These calculations also provided insight on the exchange mechanism. Seven thia-Michael CANs were synthesized from a *tris*-(trifluoromethyl)acrylate molecule containing a covalently bonded tertiary amine by reaction with a series of dithiols. The structure of the dithiols was shown to influence the chemical, thermal and mechanical properties of the resulting organic networks. CANs with T_g and storage modulus ranging from -19 °C to 25 °C and from 1.3 to 10.1 MPa, respectively, were thus prepared. The dynamic character of the thia-Michael networks was highlighted by stress relaxation and reprocessing tests. The crosslinking density and the reactivity of the thiol functions were shown to influence both the relaxation time and the flow activation energy. In particular, increasing the chain length of the crosslinker structure led to an E_a decrease. Hence, CANs with different mechanical but also dynamic properties (different reprocessing temperature) were obtained. Finally, the reprocessability of each material was examined. Lower temperatures (120 °C) were required for the reprocessing of the thiophenol-based CAN compared to the alkylthiol-based ones, which were reprocessed at 150 °C under otherwise identical conditions (1 h, 3 t). Globally, no significant change of the chemical, mechanical and thermal properties were detected as a consequence of reprocessing.

The present study highlights how the association of two different neighboring group participations provides catalyst-free thia-Michael exchange CANs. The availability of many different dithiol structures allows access to a large range of material properties. In addition, the trend relating monomer structure and flow activation energy discovered in the course of this study may be translated to other kinds of CANs.

Materials

1,3-propanedithiol (> 97%) was purchased from Fisher Scientific (Belgium, Anvers). Phthaloyl chloride (> 90%), 1-hexanol (> 99%), 2-diethylaminoethanol (> 99.5%), thiophenol (> 99%), triethanolamine

(> 98%), 4-(trifluoromethyl)thiophenol (> 95%), 1,4-butanedithiol (> 97%), 1,5-pentanedithiol (> 97%), 1,6-hexanedithiol (> 96%), 2,2'-(ethylenedioxy)diethanethiol (> 95%), pentaerythritol tetrakis(3-mercaptopropionate) (> 95%) and 4,4'-thiobisbenzenethiol (> 98%) were purchased from Sigma-Aldrich (Darmstadt Germany). 2-trifluoromethylacrylic acid (MAF) and *tert*-butyl 2-trifluoromethacrylate (MAF-TBE) were purchased form SynQuest Labs (Alachua, FL, USA). $CDCl_3$ (99.5% D) was provided by Eurisotop (Saint-Aubin, France). All materials were used as received.

Characterizations

Nuclear Magnetic Resonance

The ^1H, ^{13}C and ^{19}F NMR analyses were carried out in $CDCl_3$ using a Bruker Avance III 400 MHz NMR spectrometer at 25 °C. For ^1H NMR (400 MHz), ^{13}C NMR (101 MHz) and ^{19}F NMR (377 MHz), $CHCl_3$ served as internal standard (δ = 7.26 ppm). Data are reported as follows: chemical shift (in ppm), multiplicity (s = singlet, d = doublet, t = triplet, m = multiplet), coupling constant (in Hz), and number of nuclei from the integration. For ^{13}C and ^{19}F NMR (100 MHz), spectra were obtained with complete proton decoupling.

^1H chemical shifts are reported in delta (δ) units in parts per million (ppm) relative to the singlet at 7.26 ppm for $CDCl_3$ (residual $CHCl_3$). ^{13}C chemical shifts are reported in ppm relative to the central line of the triplet at 77.16 ppm for $CDCl_3$. ^{19}F chemical shifts are calibrated using C_6F_6 as an external standard.

Gas Chromatography – Mass spectroscopy

Gas chromatography–mass spectra (GC-MS) were recorded on a Shimadzu QP2012-SE with a Zebron ZB-5MS (20 m × 0.18 mm), capillary apolar column (stationary phase: 0.18 µm film). GC-MS method: Initial temperature: 50 °C; initial time: 2 min; ramp: 22 °C/min; final temperature: 280 °C; final time: 15 min.

High Resolution Mass Spectroscopy (HR-MS)

Mass spectroscopy (MS) analyses were recorded on a Bruker Daltonics micrOTOF-Q with an ESI source and a positive ion polarity.

Fourier Transform Infrared Spectroscopy

The IR spectra were recorded on a Nicolet 210 spectrometer, equipped with an ATR accessory. The characteristic absorptions mentioned in the text are reported in cm^{-1}.

Thermogravimetric Analyses

The thermogravimetric analyses (TGA) were carried out using a TG 209F1 apparatus (Netzch). Approximately 10 mg of sample were placed in an aluminum crucible and heated from room temperature to 580 °C at a heating rate of 20 °C/min under a nitrogen atmosphere (60 mL/min).

Differential Scanning Calorimetry

The differential scanning calorimetry (DSC) analyses were carried out using a Netzsch DSC200F3 calorimeter, which was calibrated using indium, *n*-octadecane and *n*-octane standards. Nitrogen was used as purge gas. Approximately 10 mg of sample were placed in a perforated aluminum pan and the thermal properties were recorded between -100 °C and 150 °C at 20 °C/min heating/cooling rates to observe the glass transition temperature. The T_g values were measured on the second heating ramp to erase the thermal history of the polymer.

Dynamic mechanical analyses

The dynamic mechanical analyses (DMA) were carried out on Metravib DMA 25 with Dynatest 6.8 software. The samples were tested in the uniaxial tension mode at a frequency of 1 Hz with a fixed strain of 10^{-5} m, while applying a temperature ramp at a rate of 3 °C/min from -100 °C to +150 °C. The T_α was determined as the maximum of the loss modulus E''.

Rheology

The rheology measurements were carried out on a ThermoScientific Haake Mars 60 rheometer equipped with a lower electrical temperature module and an active upper heating system, with a textured 8-mm plane-plane geometry. For all rheology experiments, the applied stress was comprised in the linear viscoelastic region. A 1 N axial force was applied to ensure proper contact between the plates and the samples for all experiments. For the stress-relaxation experiments, a 1 % torsional strain was applied on the samples, and the rubbery modulus evolution with time was monitored at different temperatures. The obtained characteristic relaxation time (τ) was used to calculate the activation energy.

Swelling index

Three samples from the same batch of the material, of ca. 20 mg each, were separately immersed in THF for 24 h. The swelling index (SI) was calculated using Equation 2, where m_2 is the mass of the swollen material and m_1 is the initial mass. Reported swelling index are average values of the three samples.

Equation 2 $$SI = \frac{m_2 - m_1}{m_1} \times 100$$

Gel content

Three samples from the same material, of around 20 mg each, were separately immersed in THF for 24 h. The samples were then dried in a ventilated oven at 70 °C for 24 h. The gel content (GC) was calculated using Equation 3, where m_2 is the mass of the dried material and m_1 is the initial mass. Reported gel content are average values of the three samples.

Equation 3 $$GC = \frac{m_2}{m_1} \times 100$$

Tensile tests

The material tensile tests were executed on an Instron 3366L5885 mechanical tester. Dog-bone sample of 10 x 2 x 1 mm were used for these analyses. The tensile speed was set at 0.1 $mm.s^{-1}$ with a 100 ms

sampling time. The Young modulus and the stress and strain at break were measured on at least five samples.

Preparation of model molecules and monomers

Trifluoromethylacryloyl chloride **1**

2-Trifluoromethylacryloyl chloride (MAF-Cl) was synthesized by the reaction of trifluoromethylacrylic acid (MAF) (29.1 g, 208 mmol) with phthaloyl dichloride (63.2 g, 311.3 mmol) at 150 °C for 2 h and then 190 °C for 30 min. The product was collected by distillation during reaction. Yield: 72 %, 23.8 g. Boiling point: 82 °C.

Hexyl (trifluoromethyl)acrylate **2**

Hexanol (1.02 g, 10 mmol, 1 eq) was dissolved in 50 mL of dichloromethane in the presence of triethylamine (1.52 g, 15 mmol, 1.5 eq). MAF-Cl (2.06 g, 13 mmol, 1.3 eq) was added dropwise at 0 °C for 10 min and the reactive mixture was stirred for 1 h at 0 °C and 4 h at 25 °C. The reaction mixture was filtered, washed once with a saturated aqueous sodium hydrogen carbonate solution, three times with distilled water and twice with brine, dried over $MgSO_4$, filtered and evaporated under reduced pressure to afford the pure hexyl (trifluoromethyl)acrylate (**2**) as a brown liquid. Yield: 75 %, 1.68 g.

^{1}H NMR (400 MHz, $CDCl_3$): δ (ppm) 6.64 (q, ^4J = 1.7 Hz, 1H, C$\underline{H_2}$-C-CF_3), 6.35 (q, ^4J = 1.3 Hz, 1H, C$\underline{H_2}$-C-CF_3), 4.18 (t, ^3J = 6.7 Hz, 2H, O-C$\underline{H_2}$-CH_2), 1.63 (m, 2H, O-CH_2-C$\underline{H_2}$-CH_2), 1.22-1.33 (m, 6H, CH_2-(C$\underline{H_2}$)$_3$-CH_3), 0.82 (t, ^3J = 7.0 Hz , 3H, CH_2-C$\underline{H_3}$).

^{19}F NMR (377 MHz, $CDCl_3$): δ (ppm) -66.7 (s).

^{13}C NMR (101 MHz, $CDCl_3$): δ (ppm) 161.4 (C$\underline{}$=O), 132.5 (q, ^3J = 5.0 Hz, C$\underline{H_2}$-C-CF_3), 131.2-132.1 (q, ^2J = 32.0 Hz, C$\underline{}$-CF_3), 117.3-125.4 (q, ^1J = 273 Hz, C$\underline{F_3}$), 66.0 (O-C$\underline{H_2}$-CH_2), 31.3 (O-CH_2-C$\underline{H_2}$), 28.3 (O-CH_2-CH_2-C$\underline{H_2}$), 25.4 (C$\underline{H_2}$-CH_2-CH_3), 22.5 (CH_2-C$\underline{H_2}$-CH_3), 13.9 (CH_2-CH_2-C$\underline{H_3}$).

HRMS (ESI+): theoretical m/z for $[M+C_3H_{10}N]^+$: 298.1988, measured: 298.1989.

2-(Diethylamino)ethyl (trifluoromethyl)acrylate **3**

2-(Diethylamino)ethanol (1.17 g, 10 mmol, 1 eq) was dissolved in 50 mL of dichloromethane in the presence of triethylamine (1.52 g, 15 mmol, 1.5 eq). MAF-Cl (2.06 g, 13 mmol, 1.3 eq) was added dropwise at 0 °C for 10 min and the reactive mixture was stirred for 1 h at 0 °C and 4 h at 25 °C. The reaction mixture was filtered, washed three times with distilled water and twice with brine, dried over $MgSO_4$, filtered and evaporated under reduced pressure to afford the pure 2-(diethylamino)ethyl (trifluoromethyl)acrylate (**3**) as a brown liquid. Yield: 68 %, 1.63 g.

^{1}H NMR (400 MHz, $CDCl_3$): δ (ppm) 6.64 (q, ^4J = 1.7 Hz, 1H, C$\underline{H_2}$-C-CF_3), 6.36 (q, ^4J = 1.3 Hz, 1H, C$\underline{H_2}$-C-CF_3), 4.25 (t, ^3J = 6.2 Hz, 2H O-C$\underline{H_2}$-CH_2), 2.71 (t, ^3J = 6.2 Hz, 2H CH_2-C$\underline{H_2}$-N), 2.51 (q, ^3J = 7.1 Hz, 4H, N-C$\underline{H_2}$-CH_3), 0.96 (t, ^3J = 7.2 Hz, 6H, N-CH_2-C$\underline{H_3}$)

^{19}F NMR (377 MHz, $CDCl_3$): δ (ppm) -66.7 (s).

^{13}C NMR (101 MHz, $CDCl_3$): δ (ppm) 161.2 (C=O), 132.6 (q, ^3J = 5.0 Hz, $\underline{C}H_2$-C-CF_3), 131.0-132.0 (q, ^2J = 32.0 Hz, $\underline{C}$-CF_3), 117.2-125.3 (q, ^1J = 273 Hz, $\underline{C}F_3$), 64.2 (O-$\underline{C}H_2$-CH_2), 50.7 (CH_2-$\underline{C}H_2$-N), 47.7 (N-$\underline{C}H_2$-CH_3), 11.9 (N-CH_2-$\underline{C}H_3$)

HRMS (ESI+): theoretical m/z for $[M+H]^+$: 240.1206, measured: 240.1208.

tert-Butyl 3,3,3-trifluoro-2-((phenylthio)methyl) propanoate **4**

In a flame-dried round-bottom flask, MAF-TBE (981 mg, 5 mmol, 1 eq.) was dissolved in DCM (10 ml). Thiophenol (551 mg, 5 mmol, 1eq.) was then added dropwise at room temperature, and the reaction was stirred for 15 min. The solvent was removed under reduced pressure and *tert*-butyl 3,3,3-trifluoro-2-((phenylthio)methyl) propanoate (**4**) was obtained as a transparent liquid. Yield > 99 %, 1.53 g.

^{1}H NMR (400 MHz, $CDCl_3$): δ (ppm) 7.18-7.35 (m, 5H, phenyl protons), 3.05-3.24 (m, 3H, S-C$\underline{H_2}$-C$\underline{H}$), 1.42 (s, 9H, C-($C\underline{H_3}$)$_3$)

^{19}F NMR (377 MHz, $CDCl_3$): δ (ppm) -69.1 (d, ^3J = 8.1 Hz)

^{13}C NMR (101 MHz, $CDCl_3$): δ (ppm) 164.9 (C=O), 127.5/129.3/131.1/133.8 (phenyl carbons), 119.8-128.2 (q, ^1J = 281 Hz, CF_3), 83.4 ($C(CH_3)_3$), 51.1-51.9 (q, ^2J = 26.7 Hz, $CH\text{-}CF_3$), 30.6 ($S\text{-}CH_2$), 27.8 ($C(CH_3)_3$).

HRMS (ESI+): theoretical m/z for $[M+H]^+$: 307.0974, measured: 307.0974.

2-(diethylamino)ethyl 3,3,3-trifluoro-2-((phenylthio)methyl) propanoate **5**

In a flame-dried round-bottom flask, compound **3** (1.19 g, 5 mmol, 1 eq.) was dissolved in DCM (10 ml). Thiophenol (551 mg, 5 mmol, 1eq.) was then added dropwise at room temperature, and the reaction was stirred for 15 min. The solvent was removed under reduced pressure and *tert*-butyl 3,3,3-trifluoro-2-((phenylthio)methyl) propanoate (**4**) was obtained as a transparent liquid. Yield > 99 %, 1.53 g.

^{1}H NMR (400 MHz, $CDCl_3$): δ (ppm) 7.16-7.35 (m, 5H, phenyl protons), 4.16-4.20 (t, ^3J = 6.3 Hz, 2H, $O\text{-}CH_2\text{-}CH_2$), 3.18-3.26 (m, 3H, $S\text{-}CH_2\text{-}CH$), 2.66 (t, ^3J = 6.3 Hz, 2H $CH_2\text{-}CH_2\text{-}N$), 2.51 (q, ^3J = 7.3 Hz, 2H, $N\text{-}CH_2\text{-}CH_3$), 0.96 (t, ^3J = 7.1 Hz, 6H, $N\text{-}CH_2\text{-}CH_3$).

^{19}F NMR (377 MHz, $CDCl_3$): δ (ppm) -68.9 (d, ^3J = 7.2 Hz).

^{13}C NMR (101 MHz, $CDCl_3$): δ (ppm) 165.9 (C=O), 133.4/131.3/129.3/127.7 (phenyl carbons), 119.6-127.2 (q, ^1J = 282 Hz, CF_3), 64.0 ($O\text{-}CH_2\text{-}CH_2$), 50.6 ($CH_2\text{-}CH_2\text{-}N$), 50.4-51.2 (q, ^2J =27.1 Hz, $CH\text{-}CF_3$), 47.4 ($N\text{-}CH_2\text{-}CH_3$), 30.5 ($S\text{-}CH_2$), 11.5 ($N\text{-}CH_2\text{-}CH_3$).

HRMS (ESI+): theoretical m/z for $[M+H]^+$: 350.1396, measured: 350.1394.

2-(diethylamino)ethyl 3-(phenylthio)propanoate **6**

In a flame-dried round-bottom flask, 2-(diethylamino)ethyl acrylate (856 mg, 5 mmol, 1 eq.) was reacted with thiophenol (551 mg, 5 mmol, 1 eq.). The mixture was stirred for 2 h at 25 °C and 2-(diethylamino)ethyl 3-(phenylthio)propanoate (**6**) was obtained as a transparent liquid. Yield > 99 %, 1.40 g.

^{1}H NMR (400 MHz, $CDCl_3$): δ (ppm) 7.18-7.38 (m, 5H, phenyl protons), 4.15 (t, ^{3}J = 6.2 Hz, O-C$\underline{H_2}$-CH_2), 3.16 (t, ^{3}J = 7.2 Hz, 2H, S-C$\underline{H_2}$-CH_2), 2.68 (t, ^{3}J = 6.2 Hz, CH_2-C$\underline{H_2}$-N), 2.64 (t, ^{3}J = 7.2 Hz, 2H, S-CH_2-C$\underline{H_2}$), 2.55 (q, ^{3}J = 7.1 Hz, 4H, N-C$\underline{H_2}$-CH_3), 1.02 (t, ^{3}J = 7.1 Hz, 6H, N-CH_2-C$\underline{H_3}$).

^{13}C NMR (101 MHz, $CDCl_3$): δ (ppm) 171.7 (C=O), 135.3/130.0/129.0/126.5 (phenyl carbons), 63.1 (O-$\underline{C}H_2$-CH_2), 51.0 (CH_2-$\underline{C}H_2$-N), 47.7 (N-$\underline{C}H_2$-CH_3), 34.4 (S-CH_2-$\underline{C}H_2$), 29.0 (S-$\underline{C}H_2$-CH_2), 12.0 (N-CH_2-$\underline{C}H_3$).

HRMS (ESI+): theoretical m/z for $[M+H]^+$: 282.1522, measured: 282.1522.

Procedure of TMCANs synthesis

Reacting **NMAF$_3$** with 1,3-propanedithiol, 1,4-butanedithiol, 1,5-pentanedithiol, 1,6-hexanedithiol, 2,2'-(ethylenedioxy)diethanethiol, pentaerythritol tetrakis(3-mercaptopropionate) and 4,4'-thiobisbenzenethiol, led to the corresponding thia-Michael CANs (**TMCANs**): **Prop-**, **But-**, **Pent-**, **Hex-**, **EDT-**, **PETMP-** and **TBT-TMCAN**. This network formation reaction was carried out in solution (50 wt% in DCM). The **TMCANs** were obtained *via* a solvent casting process (24 h at 25°C and then under vacuum at 50 °C for 10 h). The shape of the resulting materials could not be easily controlled by this method. Hence, a last curing step consisted of the shaping of the materials using a hot press. All **TMCANs** were treated at 150 °C for 1 h under 3 t, excepted for **TBT-TMCAN,** which could be shaped at 120 °C under otherwise identical conditions.

Reshaping procedure

The reprocessing behavior of the materials was examined using a Carver 3960 manual heating press. **TMCANs** were pressed at 150 °C (except for **TBT-TMCAN** which was pressed at 120 °C) for 1 h under 3 t, and then were cooled to room temperature (ca. 25°C) before removing from the hot press.

Computational details

The computational work was carried out using the Gaussian09 suite of programs.[84] The geometry optimizations were performed without any symmetry constraint using the BP86 functional and the 6-311G(d,p) basis functions for all atoms. The effects of dispersion forces (Grimme's D3 empirical

method[85]) and solvation (SMD,[86] ε = 4.5) were included during the optimization. The ZPVE, PV, and TS corrections at 298 K were obtained with Gaussian09 from the solution of the nuclear equation using the standard ideal gas and harmonic approximations at T = 298.15 K, which also verified the nature of all optimized geometries as local minima or first-order saddle points. A correction of 1.95 kcal/mol was applied to all G values to change the standard state from the gas phase (1 atm) to solution (1 M).[87]

Supporting information

^{1}H, ^{19}F and ^{13}C-NMR of **2**, **3**, **4** and **5**; ^{1}H and ^{13}C-NMR of **6**; Gibbs energy profiles; Cartesian coordinates; FTIR, TGA, DSC, DMA of initial and reshaped **TMCANs**; stress relaxations; tensile test results; reshaping pictures.

Conflict of interest

The authors declare no conflicts of interest.

Acknowledgments

This work was funded by the French National Research Agency ANR (AFCAN project: ANR-19-CE06-0014). RP is grateful to the CALMIP mesocenter of the University of Toulouse for the allocation of computational resources.

References

(1) Wadhwa, P.; Kharbanda, A.; Sharma, A. Thia-Michael Addition: An Emerging Strategy in Organic Synthesis. *Asian J. Org. Chem.* **2018**, *7* (4), 634–661. https://doi.org/10.1002/AJOC.201700609.

(2) Dunbar, K. L.; Scharf, D. H.; Litomska, A.; Hertweck, C. Enzymatic Carbon–Sulfur Bond Formation in Natural Product Biosynthesis. *Chem. Rev.* **2017**, *117* (8), 5521–5577. https://doi.org/10.1021/acs.chemrev.6b00697.

(3) Matsuno, R.; Takami, K.; Ishihara, K. Simple Synthesis of a Library of Zwitterionic Surfactants via Michael-Type Addition of Methacrylate and Alkane Thiol Compounds. *Langmuir* **2010**, *26* (16), 13028–13032. https://doi.org/10.1021/la1015466.

(4) Liu, G.; Link, J. T.; Pei, Z.; Reilly, E. B.; Leitza, S.; Nguyen, B.; Marsh, K. C.; Okasinski, G. F.; Von Geldern, T. W.; Ormes, M.; Fowler, K.; Gallatin, M. Discovery of Novel P-Arylthio Cinnamides as Antagonists of Leukocyte Function-Associated Antigen-1/Intracellular Adhesion Molecule-1 Interaction. 1. Identification of an Additional Binding Pocket Based on an Anilino Diaryl Sulfide Lead. *J. Med. Chem.* **2000**, *43* (21), 4025–4040. https://doi.org/10.1021/JM0002782.

(5) Yang, D. J.; Chen, B. Simultaneous Determination of Nonnutritive Sweeteners in Foods by HPLC/ESI-MS. *J. Agric. Food Chem.* **2009**, *57* (8), 3022–3027. https://doi.org/10.1021/JF803988U.

(6) Kade, M. J.; Burke, D. J.; Hawker, C. J. The Power of Thiol-Ene Chemistry. *J. Polym. Sci. Part A Polym. Chem.* **2010**, *48* (4), 743–750. https://doi.org/10.1002/POLA.23824.

(7) Alswieleh, A. M.; Cheng, N.; Canton, I.; Ustbas, B.; Xue, X.; Ladmiral, V.; Xia, S.; Ducker, R. E.; El Zubir, O.; Cartron, M. L.; Hunter, C. N.; Leggett, G. J.; Armes, S. P. Zwitterionic Poly(Amino Acid Methacrylate) Brushes. *J. Am. Chem. Soc.* **2014**, *136* (26), 9404–9413. https://doi.org/10.1021/ja503400r.

(8) Nair, D. P.; Podgórski, M.; Chatani, S.; Gong, T.; Xi, W.; Fenoli, C. R.; Bowman, C. N. The Thiol-Michael Addition Click Reaction: A Powerful and Widely Used Tool in Materials Chemistry. *Chem. Mater.* **2014**, *26* (1), 724–744. https://doi.org/10.1021/cm402180t.

(9) Daymon, S. P.; Miller, K. M. Probing the Dynamic and Rehealing Behavior of Crosslinked Polyester Networks Containing Thermoreversible Thiol-Michael Bonds. *Polymer (Guildf).* **2018**, *145*, 286–293. https://doi.org/10.1016/j.polymer.2018.05.009.

(10) Upadhyay, C.; Ojha, U. Stress-Induced Shape-Shifting Materials Possessing Autonomous Self-Healing and Scratch-Resistant Ability. *Chem. – An Asian J.* **2023**, *18* (4), e202201082. https://doi.org/10.1002/asia.202201082.

(11) Berne, D.; Ladmiral, V.; Leclerc, E.; Caillol, S. Thia-Michael Reaction: The Route to Promising Covalent Adaptable Networks. *Polymers (Basel).* **2022**, *14* (20), 4457. https://doi.org/10.3390/polym14204457.

(12) Chakma, P.; Digby, Z. A.; Via, J.; Shulman, M. P.; Sparks, J. L.; Konkolewicz, D. Tuning Thermoresponsive Network Materials through Macromolecular Architecture and Dynamic Thiol-Michael Chemistry. *Polym. Chem.* **2018**, *9* (38), 4744–4756. https://doi.org/10.1039/c8py00947c.

(13) M. Kharkar, P.; L. Kiick, K.; M. Kloxin, A. Design of Thiol- and Light-Sensitive Degradable Hydrogels Using Michael-Type Addition Reactions. *Polym. Chem.* **2015**, *6* (31), 5565–5574. https://doi.org/10.1039/C5PY00750J.

(14) Baldwin, A. D.; Kiick, K. L. Reversible Maleimide–Thiol Adducts Yield Glutathione-Sensitive Poly(Ethylene Glycol)–Heparin Hydrogels. *Polym. Chem.* **2012**, *4* (1), 133–143. https://doi.org/10.1039/C2PY20576A.

(15) Xiang, L.; Liu, X.; Zhang, H.; Zhao, N.; Zhang, K. Thermoresponsive Self-Healable and Recyclable Polymer Networks Based on a Dynamic Quinone Methide-Thiol Chemistry. *Polym. Chem.* **2020**, *11* (38), 6157–6162. https://doi.org/10.1039/d0py01008a.

(16) Herbert, K. M.; Dolinski, N. D.; Boynton, N. R.; Murphy, J. G.; Lindberg, C. A.; Sibener, S. J.; Rowan, S. J. Controlling the Morphology of Dynamic Thia-Michael Networks to Target Pressure-Sensitive and Hot Melt Adhesives. *ACS Appl. Mater. Interfaces* **2021**, *13* (23), 27471–27480. https://doi.org/10.1021/acsami.1c05813.

(17) Herbert, K. M.; Getty, P. T.; Dolinski, N. D.; Hertzog, J. E.; de Jong, D.; Lettow, J. H.; Romulus, J.; Onorato, J. W.; Foster, E. M.; Rowan, S. J. Dynamic Reaction-Induced Phase Separation in Tunable, Adaptive Covalent Networks. *Chem. Sci.* **2020**, *11* (19), 5028–5036. https://doi.org/10.1039/D0SC00605J.

(18) Trejo-Machin, A.; Puchot, L.; Verge, P. A Cardanol-Based Polybenzoxazine Vitrimer: Recycling, Reshaping and Reversible Adhesion. *Polym. Chem.* **2020**, *11* (44), 7026–7034.

https://doi.org/10.1039/d0py01239d.

(19) He, C.; Shi, S.; Wang, D.; Helms, B. A.; Russell, T. P. Poly(Oxime–Ester) Vitrimers with Catalyst-Free Bond Exchange. *J. Am. Chem. Soc.* **2019**, *141* (35), 13753–13757. https://doi.org/10.1021/jacs.9b06668.

(20) Majumdar, S.; Zhang, H.; Soleimani, M.; van Benthem, R. A. T. M.; Heuts, J. P. A.; Sijbesma, R. P. Phosphate Triester Dynamic Covalent Networks. *ACS Macro Lett.* **2020**, *9* (12), 1753–1758. https://doi.org/10.1021/acsmacrolett.0c00636.

(21) Huang, L.; Yang, Y.; Niu, Z.; Wu, R.; Fan, W.; Dai, Q.; He, J.; Bai, C. Catalyst-Free Vitrimer Cross-Linked by Biomass-Derived Compounds with Mechanical Robustness, Reprocessability, and Multishape Memory Effects. *Macromol. Rapid Commun.* **2021**, *42* (21), 2100432. https://doi.org/10.1002/MARC.202100432.

(22) Lessard, J. J.; Garcia, L. F.; Easterling, C. P.; Sims, M. B.; Bentz, K. C.; Arencibia, S.; Savin, D. A.; Sumerlin, B. S. Catalyst-Free Vitrimers from Vinyl Polymers. *Macromolecules* **2019**, *52* (5), 2105–2111. https://doi.org/10.1021/acs.macromol.8b02477.

(23) Debnath, S.; Kaushal, S.; Ojha, U. Catalyst-Free Partially Bio-Based Polyester Vitrimers. *ACS Appl. Polym. Mater.* **2020**, *2* (2), 1006–1013. https://doi.org/10.1021/acsapm.0c00016.

(24) Cuminet, F.; Caillol, S.; Dantras, É.; Leclerc, É.; Ladmiral, V. Neighboring Group Participation and Internal Catalysis Effects on Exchangeable Covalent Bonds: Application to the Thriving Field of Vitrimer Chemistry. *Macromolecules* **2021**, *54* (9), 3927–3961. https://doi.org/10.1021/acs.macromol.0c02706.

(25) Guerre, M.; Taplan, C.; Winne, J. M.; Du Prez, F. E. Vitrimers: Directing Chemical Reactivity to Control Material Properties. *Chem. Sci.* **2020**, *11* (19), 4855–4870. https://doi.org/10.1039/D0SC01069C.

(26) Liu, M.; Zhong, J.; Li, Z.; Rong, J.; Yang, K.; Zhou, J.; Shen, L.; Gao, F.; Huang, X.; He, H. A High Stiffness and Self-Healable Polyurethane Based on Disulfide Bonds and Hydrogen Bonding. *Eur. Polym. J.* **2020**, *124*, 109475. https://doi.org/10.1016/j.eurpolymj.2020.109475.

(27) Altuna, F.; Hoppe, C.; Williams, R. Epoxy Vitrimers: The Effect of Transesterification Reactions on the Network Structure. *Polymers (Basel).* **2018**, *10* (1), 43. https://doi.org/10.3390/polym10010043.

(28) Liu, W.; Schmidt, D. F.; Reynaud, E. Catalyst Selection, Creep, and Stress Relaxation in High-Performance Epoxy Vitrimers. *Ind. Eng. Chem. Res.* **2017**, *56* (10), 2667–2672. https://doi.org/10.1021/acs.iecr.6b03829.

(29) Chen, M.; Zhou, L.; Chen, Z.; Zhang, Y.; Xiao, P.; Yu, S.; Wu, Y.; Zhao, X. Multi-Functional Epoxy Vitrimers: Controllable Dynamic Properties, Multiple-Stimuli Response, Crack-Healing and Fracture-Welding. *Compos. Sci. Technol.* **2022**, *221*, 109364. https://doi.org/10.1016/J.COMPSCITECH.2022.109364.

(30) Montarnal, D.; Capelot, M.; Tournilhac, F.; Leibler, L. Silica-Like Malleable Materials from Permanent Organic Networks. *Science (80-.).* **2011**, *334* (6058), 965–968. https://doi.org/10.1126/science.1212648.

(31) Wang, S.; Teng, N.; Dai, J.; Liu, J.; Cao, L.; Zhao, W.; Liu, X. Taking Advantages of Intramolecular Hydrogen Bonding to Prepare Mechanically Robust and Catalyst-Free Vitrimer. *Polymer (Guildf).* **2020**, *210*, 123004. https://doi.org/10.1016/j.polymer.2020.123004.

(32) Delahaye, M.; Tanini, F.; Holloway, J. O.; Winne, J. M.; Du Prez, F. E. Double Neighbouring Group

Participation for Ultrafast Exchange in Phthalate Monoester Networks. *Polym. Chem.* **2020**, *11* (32), 5207–5215. https://doi.org/10.1039/d0py00681e.

(33) Delahaye, M.; Winne, J. M.; Du Prez, F. E. Internal Catalysis in Covalent Adaptable Networks: Phthalate Monoester Transesterification As a Versatile Dynamic Cross-Linking Chemistry. *J. Am. Chem. Soc.* **2019**, *141* (38), 15277–15287. https://doi.org/10.1021/jacs.9b07269.

(34) Zhang, H.; Majumdar, S.; Van Benthem, R. A. T. M.; Sijbesma, R. P.; Heuts, J. P. A. Intramolecularly Catalyzed Dynamic Polyester Networks Using Neighboring Carboxylic and Sulfonic Acid Groups. *ACS Macro Lett.* **2020**, *12*, 272–277. https://doi.org/10.1021/acsmacrolett.9b01023.

(35) Van Lijsebetten, F.; Spiesschaert, Y.; Winne, J. M.; Du Prez, F. E. Reprocessing of Covalent Adaptable Polyamide Networks through Internal Catalysis and Ring-Size Effects. *J. Am. Chem. Soc.* **2021**, *143* (38), 15834–15844. https://doi.org/10.1021/jacs.1c07360.

(36) Chen, Y.; Zhang, H.; Majumdar, S.; van Benthem, R. A. T. M.; Heuts, J. P. A.; Sijbesma, R. P. Dynamic Polyamide Networks via Amide–Imide Exchange. *Macromolecules* **2021**, *54* (20), 9703–9711. https://doi.org/10.1021/acs.macromol.1c01389.

(37) Han, J.; Liu, T.; Zhang, S.; Hao, C.; Xin, J.; Guo, B.; Zhang, J. Hyperbranched Polymer Assisted Curing and Repairing of an Epoxy Coating. *Ind. Eng. Chem. Res.* **2019**, *58* (16), 6466–6475. https://doi.org/10.1021/acs.iecr.9b00800.

(38) Liu, T.; Zhang, S.; Hao, C.; Verdi, C.; Liu, W.; Liu, H.; Zhang, J. Glycerol Induced Catalyst-Free Curing of Epoxy and Vitrimer Preparation. *Macromol. Rapid Commun.* **2019**, *40* (7), 1800889. https://doi.org/10.1002/marc.201800889.

(39) Mu, S.; Zhang, Y.; Zhou, J.; Wang, B.; Wang, Z. Recyclable and Mechanically Robust Palm Oil-Derived Epoxy Resins with Reconfigurable Shape-Memory Properties. *ACS Sustain. Chem. Eng.* **2020**, *8* (13), 5296–5304. https://doi.org/10.1021/acssuschemeng.0c00443.

(40) Altuna, F. I.; Hoppe, C. E.; Williams, R. J. J. Shape Memory Epoxy Vitrimers Based on DGEBA Crosslinked with Dicarboxylic Acids and Their Blends with Citric Acid. *RSC Adv.* **2016**, *6* (91), 88647–88655. https://doi.org/10.1039/c6ra18010h.

(41) Altuna, F. I.; Pettarin, V.; Williams, R. J. J. Self-Healable Polymer Networks Based on the Cross-Linking of Epoxidised Soybean Oil by an Aqueous Citric Acid Solution. *Green Chem.* **2013**, *15* (12), 3360. https://doi.org/10.1039/c3gc41384e.

(42) Liu, W.-X.; Zhang, C.; Zhang, H.; Zhao, N.; Yu, Z.-X.; Xu, J. Oxime-Based and Catalyst-Free Dynamic Covalent Polyurethanes. *J. Am. Chem. Soc.* **2017**, *139* (25), 8678–8684. https://doi.org/10.1021/jacs.7b03967.

(43) Shi, J.; Zheng, T.; Zhang, Y.; Guo, B.; Xu, J. Reprocessable Cross-Linked Polyurethane with Dynamic and Tunable Phenol–Carbamate Network. *ACS Sustain. Chem. Eng.* **2020**, *8* (2), 1207–1218. https://doi.org/10.1021/acssuschemeng.9b06435.

(44) Fujita, N.; Shinkai, S.; James, T. D. Boronic Acids in Molecular Self-Assembly. *Chem. – An Asian J.* **2008**, *3* (7), 1076–1091. https://doi.org/10.1002/ASIA.200800069.

(45) Marco-Dufort, B.; Tibbitt, M. W. Design of Moldable Hydrogels for Biomedical Applications Using Dynamic Covalent Boronic Esters. *Mater. Today Chem.* **2019**, *12*, 16–33. https://doi.org/10.1016/j.mtchem.2018.12.001.

(46) Spiesschaert, Y.; Taplan, C.; Stricker, L.; Guerre, M.; Winne, J. M.; Du Prez, F. E. Influence of the Polymer Matrix on the Viscoelastic Behaviour of Vitrimers. *Polym. Chem.* **2020**, *11* (33), 5377–

5385. https://doi.org/10.1039/d0py00114g.

(47) Long, K. F.; Wang, H.; Dimos, T. T.; Bowman, C. N. Effects of Thiol Substitution on the Kinetics and Efficiency of Thiol-Michael Reactions and Polymerizations. *Macromolecules* **2021**, *54* (7), 3093–3100. https://doi.org/10.1021/acs.macromol.0c02677.

(48) Long, K. F.; Bongiardina, N. J.; Mayordomo, P.; Olin, M. J.; Ortega, A. D.; Bowman, C. N. Effects of 1°, 2°, and 3° Thiols on Thiol–Ene Reactions: Polymerization Kinetics and Mechanical Behavior. *Macromolecules* **2020**, *53* (14), 5805–5815. https://doi.org/10.1021/acs.macromol.0c00369.

(49) Li, Y.; Liu, T.; Zhang, S.; Shao, L.; Fei, M.; Yu, H.; Zhang, J. Catalyst-Free Vitrimer Elastomers Based on a Dimer Acid: Robust Mechanical Performance, Adaptability and Hydrothermal Recyclability. *Green Chem.* **2020**, *22* (3), 870–881. https://doi.org/10.1039/c9gc04080c.

(50) Altuna, F. I.; Casado, U.; Dell'Erba, I. E.; Luna, L.; Hoppe, C. E.; Williams, R. J. J. Epoxy Vitrimers Incorporating Physical Crosslinks Produced by Self-Association of Alkyl Chains. *Polym. Chem.* **2020**, *11* (7), 1337–1347. https://doi.org/10.1039/C9PY01787A.

(51) Giebler, M.; Sperling, C.; Kaiser, S.; Duretek, I.; Schlögl, S. Epoxy-Anhydride Vitrimers from Aminoglycidyl Resins with High Glass Transition Temperature and Efficient Stress Relaxation. *Polymers (Basel).* **2020**, *12* (5), 1148. https://doi.org/10.3390/polym12051148.

(52) Altuna, F. I.; Hoppe, C. E.; Williams, R. J. J. Epoxy Vitrimers with a Covalently Bonded Tertiary Amine as Catalyst of the Transesterification Reaction. *Eur. Polym. J.* **2019**, *113*, 297–304. https://doi.org/10.1016/j.eurpolymj.2019.01.045.

(53) Liu, T.; Hao, C.; Shao, L.; Kuang, W.; Cosimbescu, L.; Simmons, K. L.; Zhang, J. Carbon Fiber Reinforced Epoxy Vitrimer: Robust Mechanical Performance and Facile Hydrothermal Decomposition in Pure Water. *Macromol. Rapid Commun.* **2021**, *42* (3), 2000458. https://doi.org/10.1002/marc.202000458.

(54) Hao, C.; Liu, T.; Zhang, S.; Liu, W.; Shan, Y.; Zhang, J. Triethanolamine-Mediated Covalent Adaptable Epoxy Network: Excellent Mechanical Properties, Fast Repairing, and Easy Recycling. *Macromolecules* **2020**, *53* (8), 3110–3118. https://doi.org/10.1021/acs.macromol.9b02243.

(55) Ehbets, J.; Lorenzen, S.; Mahler, C.; Bertermann, R.; Berkefeld, A.; Poater, J.; Fritz-Langhals, E.; Weidner, R.; Bickelhaupt, F. M.; Tacke, R. Synthesis and Hydrolysis of Alkoxy(Aminoalkyl)Diorganylsilanes of the Formula Type R 2 (RO)Si(CH 2) n NH 2 (R = Alkyl, n = 1–3): A Systematic Experimental and Computational Study. *Eur. J. Inorg. Chem.* **2016**, *2016* (11), 1641–1659. https://doi.org/10.1002/ejic.201600077.

(56) Nishimura, Y.; Chung, J.; Muradyan, H.; Guan, Z. Silyl Ether as a Robust and Thermally Stable Dynamic Covalent Motif for Malleable Polymer Design. *J. Am. Chem. Soc.* **2017**, *139* (42), 14881–14884. https://doi.org/10.1021/jacs.7b08826.

(57) Zych, A.; Pinalli, R.; Soliman, M.; Vachon, J.; Dalcanale, E. Polyethylene Vitrimers via Silyl Ether Exchange Reaction. *Polymer (Guildf).* **2020**, *199*, 122567. https://doi.org/10.1016/j.polymer.2020.122567.

(58) Yamawake, K.; Hayashi, M. The Role of Tertiary Amines as Internal Catalysts for Disulfide Exchange in Covalent Adaptable Networks. *Polym. Chem.* **2023**, *14* (6), 680–686. https://doi.org/10.1039/D2PY01406H.

(59) Cromwell, O. R.; Chung, J.; Guan, Z. Malleable and Self-Healing Covalent Polymer Networks through Tunable Dynamic Boronic Ester Bonds. *J. Am. Chem. Soc.* **2015**, *137* (20), 6492–6495. https://doi.org/10.1021/jacs.5b03551.

(60) Matějka, L.; Dušek, K. Specific Features of the Kinetics of Addition Esterification of Epoxide with the Carboxyl Group. *Polym. Bull.* **1986**, *15* (3), 215–221. https://doi.org/10.1007/BF00255065.

(61) Hoppe, C. E.; Galante, M. J.; Oyanguren, P. A.; Williams, R. J. J. Epoxies Modified by Palmitic Acid: From Hot-Melt Adhesives to Plasticized Networks. *Macromol. Mater. Eng.* **2005**, *290* (5), 456–462. https://doi.org/10.1002/mame.200400348.

(62) Dusek, K.; Matejka, L. Transesterification and Gelation of Polyhydroxy Esters Formed from Diepoxides and Dicarboxylic Acids. *Adv. Chem. Ser.* **1984**, 15–26. https://doi.org/10.1021/ba-1984-0208.ch002.

(63) Berne, D.; Cuminet, F.; Lemouzy, S.; Joly-Duhamel, C.; Poli, R.; Caillol, S.; Leclerc, E.; Ladmiral, V. Catalyst-Free Epoxy Vitrimers Based on Transesterification Internally Activated by an α–CF 3 Group. *Macromolecules* **2022**, *55* (5), 1669–1679. https://doi.org/10.1021/acs.macromol.1c02538.

(64) Cuminet, F.; Berne, D.; Lemouzy, S.; Dantras, E.; Joly-Duhamel, C.; Caillol, S.; Leclerc, E.; Ladmiral, V. Catalyst-Free Transesterification Vitrimers: Activation via α -Difluoroesters. *Polym. Chem.* **2022**, *8*, 5255–5446. https://doi.org/10.1039/D2PY00124A.

(65) Berne, D.; Tanguy, G.; Caillol, S.; Poli, R.; Ladmiral, V.; Leclerc, E. Transamidation Vitrimers Enabled by Neighbouring Fluorine Atom Activation. *Polym. Chem.* **2023**. https://doi.org/10.1039/D3PY00577A.

(66) Berne, D.; Quienne, B.; Caillol, S.; Leclerc, E.; Ladmiral, V. Biobased Catalyst-Free Covalent Adaptable Networks Based on CF 3 -Activated Synergistic Aza-Michael Exchange and Transesterification. *J. Mater. Chem. A* **2022**, *10* (47), 25085–25097. https://doi.org/10.1039/D2TA05067F.

(67) Berne, D.; Lemouzy, S.; Guiffrey, P.; Caillol, S.; Ladmiral, V.; Manoury, E.; Poli, R.; Leclerc, E. Catalyst-Free Thia-Michael Addition to A-Trifluoromethylacrylates for 3D Network Synthesis. *Chem. – A Eur. J.* **2023**, e202203712. https://doi.org/10.1002/chem.202203712.

(68) Berne, D.; Caillol, S.; Ladmiral, V.; Leclerc, E. Synthesis of Polyester Thermosets via Internally Catalyzed Michael-Addition of Methylene Compounds on a 2-(Trifluoromethyl)Acrylate-Derived Building Block. *Eur. Polym. J.* **2022**, *175*, 111362. https://doi.org/10.1016/j.eurpolymj.2022.111362.

(69) Cuminet, F.; Lemouzy, S.; Dantras, É.; Leclerc, É.; Ladmiral, V.; Caillol, S. From Vineyards to Reshapable Materials: α-CF 2 Activation in 100% Resveratrol-Based Catalyst-Free Vitrimers. *Polym. Chem.* **2023**, *14* (12), 1387–1395. https://doi.org/10.1039/D3PY00017F.

(70) Cuminet, F.; Caillol, S.; Dantras, É.; Leclerc, É.; Lemouzy, S.; Totée, C.; Guille, O.; Ladmira, V. Synthesis of a Transesterification Vitrimer Activated by Fluorine from an α,α-Difluoro Carboxylic Acid and a Diepoxy. *Eur. Polym. J.* **2022**, 111718. https://doi.org/10.1016/J.EURPOLYMJ.2022.111718.

(71) Lemouzy, S.; Cuminet, F.; Berne, D.; Caillol, S.; Ladmiral, V.; Poli, R.; Leclerc, E. Understanding the Reshaping of Fluorinated Polyester Vitrimers by Kinetic and DFT Studies of the Transesterification Reaction. *Chem. – A Eur. J.* **2022**, *28* (48). https://doi.org/10.1002/chem.202201135.

(72) Zhang, B.; Chakma, P.; Shulman, M. P.; Ke, J.; Digby, Z. A.; Konkolewicz, D. Probing the Mechanism of Thermally Driven Thiol-Michael Dynamic Covalent Chemistry. *Org. Biomol. Chem.* **2018**, *16* (15), 2725–2734. https://doi.org/10.1039/c8ob00397a.

(73) Wang, T.; Wang, J.; He, X.; Cao, Z.; Xu, D.; Gao, F.; Zhong, J.; Shen, L. An Ambient Curable Coating

Material Based on the Michael Addition Reaction of Acetoacetylated Castor Oil and Multifunctional Acrylate. *Coatings* **2019**, *9* (1), 37. https://doi.org/10.3390/coatings9010037.

(74) Elling, B. R.; Dichtel, W. R. Reprocessable Cross-Linked Polymer Networks: Are Associative Exchange Mechanisms Desirable? *ACS Cent. Sci.* **2020**, *6* (9), 1488–1496. https://doi.org/10.1021/acscentsci.0c00567.

(75) Zhang, G.; Zhao, Q.; Yang, L.; Zou, W.; Xi, X.; Xie, T. Exploring Dynamic Equilibrium of Diels–Alder Reaction for Solid State Plasticity in Remoldable Shape Memory Polymer Network. *ACS Macro Lett.* **2016**, *5* (7), 805–808. https://doi.org/10.1021/acsmacrolett.6b00357.

(76) Kuang, X.; Liu, G.; Dong, X.; Wang, D. Correlation between Stress Relaxation Dynamics and Thermochemistry for Covalent Adaptive Networks Polymers. *Mater. Chem. Front.* **2017**, *1* (1), 111–118. https://doi.org/10.1039/c6qm00094k.

(77) Hayashi, M.; Chen, L. Functionalization of Triblock Copolymer Elastomers by Cross-Linking the End Blocks via Trans-N -Alkylation-Based Exchangeable Bonds. *Polym. Chem.* **2020**, *11* (10), 1713–1719. https://doi.org/10.1039/C9PY01759C.

(78) Taplan, C.; Guerre, M.; Du Prez, F. E. Covalent Adaptable Networks Using β-Amino Esters as Thermally Reversible Building Blocks. *J. Am. Chem. Soc.* **2021**, *143* (24), 9140–9150. https://doi.org/10.1021/jacs.1c03316.

(79) Berne, D.; Coste, G.; Morales-Cerrada, R.; Boursier, M.; Pinaud, J.; Ladmiral, V.; Caillol, S. Taking Advantage of β-Hydroxy Amine Enhanced Reactivity and Functionality for the Synthesis of Dual Covalent Adaptable Networks. *Polym. Chem.* **2022**, *13* (25), 3806–3814. https://doi.org/10.1039/d2py00274d.

(80) Breuillac, A.; Kassalias, A.; Nicolaÿ, R. Polybutadiene Vitrimers Based on Dioxaborolane Chemistry and Dual Networks with Static and Dynamic Cross-Links. *Macromolecules* **2019**, *52* (18), 7102–7113. https://doi.org/10.1021/acs.macromol.9b01288.

(81) Gablier, A.; Saed, M. O.; Terentjev, E. M. Rates of Transesterification in Epoxy-Thiol Vitrimers. *Soft Matter* **2020**, *16* (22), 5195–5202. https://doi.org/10.1039/d0sm00742k.

(82) Hayashi, M.; Yano, R.; Takasu, A. Synthesis of Amorphous Low: T g Polyesters with Multiple COOH Side Groups and Their Utilization for Elastomeric Vitrimers Based on Post-Polymerization Cross-Linking. *Polym. Chem.* **2019**, *10* (16), 2047–2056. https://doi.org/10.1039/c9py00293f.

(83) Shi, Y.; Liu, X.; Cao, H.; Bie, F.; Han, Y.; Yan, P.; Szostak, R.; Szostak, M.; Liu, C. Conversion of Esters to Thioesters under Mild Conditions. *Org. Biomol. Chem.* **2021**, *19* (13), 2991–2996. https://doi.org/10.1039/D1OB00187F.

(84) Frisch, M. J.; Trucks, G. W.; Schlegel, H. B.; Scuseria, G. E.; Robb, M. A.; Cheeseman, J. R.; Scalmani, G.; Barone, V.; Mennucci, B.; Petersson, G. A.; Nakatsuji, H.; Caricato, M.; Li, X.; Hratchian, H. P.; Izmaylov, A. F.; Bloino, J.; Zheng, G.; Sonnenberg, J. L.; Hada, M.; Ehara, M.; Toyota, K.; Fukuda, R.; Hasegawa, J.; Ishida, M.; Nakajima, T.; Honda, Y.; Kitao, O.; Nakai, H.; Vreven, T.; Montgomery, J. A.; Peralta, J. E.; Ogliaro, F.; Bearpark, M.; Heyd, J. J.; Brothers, E.; Kudin, K. N.; Staroverov, V. N.; Kobayashi, R.; Normand, J.; Raghavachari, K.; Rendell, A.; Burant, J. C.; Iyengar, S. S.; Tomasi, J.; Cossi, M.; Rega, N.; Millam, J. M.; Klene, M.; Knox, J. E.; Cross, J. B.; Bakken, V.; Adamo, C.; Jaramillo, J.; Gomperts, R.; Stratmann, R. E.; Yazyev, O.; Austin, A. J.; Cammi, R.; Pomelli, C.; Ochterski, J. W.; Martin, R. L.; Morokuma, K.; Zakrzewski, V. G.; Voth, G. A.; Salvador, P.; Dannenberg, J. J.; Dapprich, S.; Daniels, A. D.; Farkas; Foresman, J. B.; Ortiz, J. V; Cioslowski, J.; Fox, D. J. Gaussian 09, Revision B.01. *Gaussian 09, Revision B.01, Gaussian, Inc., Wallingford CT*. 2009.

(85) Grimme, S.; Antony, J.; Ehrlich, S.; Krieg, H. A Consistent and Accurate Ab Initio Parametrization of Density Functional Dispersion Correction (DFT-D) for the 94 Elements H-Pu. *J. Chem. Phys.* **2010**, *132* (15), 154104. https://doi.org/10.1063/1.3382344.

(86) Marenich, A. V.; Cramer, C. J.; Truhlar, D. G. Universal Solvation Model Based on Solute Electron Density and on a Continuum Model of the Solvent Defined by the Bulk Dielectric Constant and Atomic Surface Tensions. *J. Phys. Chem. B* **2009**, *113* (18), 6378–6396. https://doi.org/10.1021/jp810292n.

(87) Bryantsev, V. S.; Diallo, M. S.; Goddard, W. A. Calculation of Solvation Free Energies of Charged Solutes Using Mixed Cluster/Continuum Models. *J. Phys. Chem. B* **2008**, *112* (32), 9709–9719. https://doi.org/10.1021/jp802665d.